



Norwegian University
of Life Sciences

Master's Thesis 2018 30 ECTS

Faculty of Science and Technology
Espen Olsen

Study on the Cooling Effect for Floating PV Modules in Thermal Contact with Water and the Potential for Modelling Floating PV

Ida Hugem Lereng

Industrial Economics and Technology Management
Faculty of Science and Technology

Preface

This thesis marks the completion of a five-year Master of Science degree in Industrial Economics and Technology Management (Industriell Økonomi) at the Norwegian University of Life Sciences (NMBU). The thesis is based on an initiative from the Institute for Energy Technology (IFE), in collaboration with Ocean Sun.

First and foremost, I want to thank my supervisor at IFE, Josefine Selj, for giving me invaluable advice and great support throughout this semester. I also want to thank my supervisor at NMBU, Espen Olsen, for introducing me to IFE and for providing me with great advice and motivation.

Furthermore, I would like to thank Jonathan Fagerström for his enthusiasm in helping me with TRNSYS, Mari Benedikte Øgaard and Åsmund Skomedal for helping me set up and run the experiment at IFE and Bjørn Aarseth for helping with the IR camera and picture taking. Furthermore, I want to thank Hallvard Gustav Fjær for helping me develop a thermal model and Børge Bjørneklett, my contact person in Ocean Sun, for answering all questions related to their concept and the experiment in Singapore.

Lastly, I would like to thank my boyfriend, parents and friends for continuous support throughout this semester.

Kjeller, 10.05.2018

Ida Hugem Lereng

Abstract

Floating solar power has become an increasingly popular technology, mainly because it does not occupy land areas and because lower operational temperatures lead to higher power outputs. With 75 % of the world's surface consisting of water and a demand for more renewable energy production, the potential for solar PV increases significantly.

The purpose of this study is to quantify the cooling effect for a floating PV module in thermal contact with water. The cooling effect is estimated through analysis of experimental data from a test site at IFE, where the temperatures and power output of a floating module is measured. The data from the floating module is compared to measured data from a reference module. Additionally, a thermal model has been developed, aimed at estimating the temperature and power output for a floating module. Simulation software programs, PVsyst and TRNSYS, were also evaluated in terms of their ability to simulate floating PV modules.

For the test period (10.04.2018 – 15.04.2018) and time interval during those days (11.15 – 16.00), the results indicate that the floating module has approximately 2-6 % higher normalized power output than the reference module. The back-surface temperature of the floating module is approximately 6-7°C lower than the reference temperature. The results also indicate that the difference in performance and temperature increases when irradiance and ambient temperature increase.

Furthermore, the experimental results suggest that the cooling effect of the floating module varies greatly throughout a day, between approximately 60-110 W/m²K. The cooling effect for the reference module seems to be more stationary, ranging around 40-50 W/m²K. Additionally, the cooling effect seem to increase at higher ambient temperature and irradiance. However, some of the materials used in the experiment are not applicable for offshore installations, so suitable materials might lead to different cooling effects for other installations.

The thermal model developed proved to underestimate both power output and module temperature, which seem to mainly be due to not including heat capacities in the model. PVsyst seems to be the best software suited to simulate floating PV, as the cooling effect can be given as a parameter. However, none of the simulation software programs are fully capable of modeling floating PV, due to limited features necessary for such installations.

Sammendrag

Flytende solenergi er en teknologi som stadig blir mer populær, hovedsakelig fordi flytende installasjoner ikke krever landareal, samt fordi lavere driftstemperaturer fører til høyere effekt. Ettersom 75 % av verdens overflate består av vann og behovet for fornybar energi øker, øker dermed også potensialet for solenergi.

Formålet med denne oppgaven er å kvantifisere kjøleeffekten til en flytende solcellemodul i termisk kontakt med vann. Kjøleeffekten estimeres ved analyse av eksperimentell data fra et testanlegg på IFE, hvor modulens temperatur og effekt måles. Dataene sammenlignes også med målte data fra en referansemodul. I tillegg har en termisk modell blitt utviklet for å estimere temperatur og effekt for flytende moduler. Simuleringsprogrammene PVsyst og TRNSYS ble brukt for å modellere flytende PV, og deres evne til dette ble så evaluert.

Resultatene fra testperioden (10.04.18 – 15.04.18) og tidsintervallet (11.15 – 16.00) for testperioden indikerer at den flytende modulen har omtrent 2-6 % høyere normalisert effekt sammenlignet med referansemodulen. Temperaturen på baksiden av den flytende modulen er målt til å være omtrent 6-7°C lavere enn referansemodulen. Resultatene indikerer også at differansen i ytelse og temperatur øker når solinnstrålingen og omgivelsestemperaturen øker.

Videre antyder de eksperimentelle resultatene at kjøleeffekten til den flytende modulen varierer i løpet av en dag, mellom om lag 60-110 W/m²K. Kjøleeffekten for referansemodulen virker å være mer stabil, rundt 40-50 W/m²K. Det ser ut til at kjøleeffekten øker ved høyere omgivelsestemperaturer og innstråling. Materialene som ble brukt i eksperimentet er ikke egnet for offshore installasjoner, så andre installasjoner vil sannsynligvis gi andre kjøleverdier.

Den termiske modellen viste seg å underestimere både effekt og modultemperatur, som tilsynelatende kan forklares av at varmekapasitet ikke er inkludert i modellen. Videre antas PVsyst å være programvaren best egnet til å simulere flytende solcellemoduler, da kjøleeffekten kan gis som en parameter for simuleringen. Likevel argumenteres det for at ingen av simuleringsprogrammene er fullstendig egnet til å modellere flytende PV, grunnet begrensede funksjoner.

Nomenclature

Symbols

A	Area	m^2
c	Specific heat capacity	$J/kg \cdot K$
E	Energy	J
FF	Fill factor	-
G_{hor}	Global horizontal irradiance	W/m^2
h	Convective heat coefficient	W/m^2K
I	Current	A
I_L	Solar irradiance	W/m^2
I_{L0}	Reference solar irradiance	W/m^2
k	Thermal conductivity	$W/m \cdot K$
L	Length	m
Nu	Nusselt number	-
P	Power	W
P_n	Normalized power output	-
P_{max}	Maximum power point, from flash test	W
$P_{measured}$	Measured power output from PV module	W
PR	Performance ratio	%
Pr	Prandlt number	-
Q	Heat flux	W
R	Thermal resistance	K/W
R_S	Series resistance	Ω
R_P	Shunt resistance	Ω
Re	Reynold number	-
T	Temperature	$^{\circ}C$
T_s	Temperature of a surface	$^{\circ}C$
U	Thermal loss factor	W/m^2K
v	Wind speed	m/s
ν_k	Kinematic viscosity	m^2/s
V	Voltage	V
α	Solar altitude angle	$^{\circ}$
β	Temperature coefficient for P_{MPP}	$\%/^{\circ}C$

β_{th}	Thermal expansion coefficient	K^{-1}
μ	Dynamic viscosity	$kg/m \cdot s$
η	Efficiency	%
ρ	Density	kg/m^3
ν	Frequency	Hz
θ	Zenith angle / Angle of incidence	$^{\circ}$

Abbreviations

<i>AM</i>	Air mass
<i>FPV</i>	Floating photovoltaic
<i>LCOE</i>	Levelized cost of electricity
<i>NOCT</i>	Nominal operating cell temperature
<i>O&M</i>	Operation and Maintenance
<i>PV</i>	Photovoltaic
<i>STC</i>	Standard test conditions

Subscripts

<i>amb</i>	Ambient
<i>b</i>	Back side (of PV)
<i>c</i>	Cell
<i>C</i>	Conduction band
<i>f</i>	Front side (of PV)
<i>G</i>	Bandgap
<i>in</i>	Input
<i>m</i>	Module (back surface)
<i>MPP</i>	Max power point
<i>OC</i>	Open circuit
<i>out</i>	Output
<i>ph</i>	Photon
<i>SC</i>	Short circuit
<i>STC</i>	Standard test conditions
<i>V</i>	Valence band
<i>water</i>	Water
∞	Infinity

Constants

g	Gravity constant	9.806 65 m/s ²
h	Planck constant	6.626 069 x 10 ⁻³⁴ Js
k_B	Boltzmann constant	1.380 649 x 10 ⁻²³ JK ⁻¹
q	Elementary charge	1.602 x 10 ⁻¹⁹ C

Table of Contents

Preface	I
Abstract.....	III
Sammendrag	V
Nomenclature.....	VII
1 Introduction.....	1
1.1 Background.....	1
1.2 Objective	2
2 Theory.....	3
2.1 The sun	3
2.1.1 Air Mass and angle of incidence	3
2.1.2 Solar irradiance and solar insolation	4
2.1.3 Albedo effect.....	4
2.2 Angles for PV-installations.....	4
2.3 Photovoltaic theory	5
2.3.1 Generation of electricity	5
2.3.2 Solar cell parameters	6
2.3.3 The two-diode model.....	7
2.3.4 Solar cell efficiency.....	8
2.3.5 Solar cell technologies	9
2.3.6 Performance ratio	10
2.4 Heat transfer	10
2.4.1 Thermal loss factor	11
2.4.2 Convection	12
2.4.3 Conduction.....	13
2.4.4 Radiation.....	13
2.5 Floating PV.....	13
2.5.1 Operational temperature of floating PV.....	14
2.5.2 Costs of floating PV	14
2.5.3 Current installations.....	15
2.5.4 Ocean Sun's concept	18
3 Method.....	19
3.1 Test station: IFE, Kjeller	19
3.1.1 Layout and surroundings	19
3.1.2 Insolation and temperature at the test site.....	20
3.1.3 Measurements at test station	21
3.2 Test station: Singapore	26

3.2.1	Layout and surroundings	26
3.2.2	Insolation and temperature at the test site	28
3.3	Data analysis	28
3.3.1	Data selection	28
3.3.2	Data adjustment	30
3.3.3	Presentation of results	32
3.3.4	Summary of data analysis	32
3.4	Mathematical methodology	32
3.4.1	Background	33
3.4.2	Structural setup	34
3.4.3	Parameters	34
3.4.4	Presentation of results and summary	36
3.5	Computational methodology	36
3.5.1	PVsys	37
3.5.2	TRNSYS	39
3.6	Summary of methodologies	40
4	Results and discussion	41
4.1	Experimental results from IFE, Kjeller	41
4.1.1	Performance	41
4.1.2	Back-surface module temperature	43
4.1.3	U-value	47
4.1.4	Summary	48
4.2	Estimated results from the thermal model	49
4.3	Results from computer simulations	52
4.3.1	PVsys	52
4.3.2	TRNSYS	54
4.3.3	Comparison of simulated and experimental results	56
5	Conclusions	59
6	Further work	61
	References	63
	Appendix	67
	Appendix A	68
	Appendix B	73

1 Introduction

1.1 Background

From 1973 to 2015, the world energy supply and consumption more than doubled, consumption of electricity almost tripled and CO₂ emissions doubled (IEA, 2017). Emissions from the energy sector account for two-thirds of the greenhouse gas emissions and 80 % of CO₂ emissions (IEA, 2018).

Scientists have proven that emissions of greenhouse gases lead to climate change, and that these changes are mainly caused by anthropogenic actions (UNFCCC, 2018a).

At the United Nations for Climate Change Conference in Paris in 2015, COP21, a bottom-up approach to reduce emissions was decided, popularly known as the “Paris agreement”. The overall goal of the Paris agreement is to prevent the global temperature to increase above 2°C compared to pre-industrial levels, while pursuing to limit the increase to 1.5°C (UNFCCC, 2018b).

To achieve the goal of the Paris agreement, approximately 40 % of the CO₂ emissions must be reduced (IEA, 2017). To achieve this, and keep up with the increasing electricity demand, renewable energy technologies are required to increase their production. From 1973 to 2015, the electricity generation from non-hydro renewables (solar, wind geothermal, tidal, waves, biofuels, waste, heat and other), increased from 0.6 % to 7.1 % of the total electricity generation.

The solar photovoltaic (PV) market is, according to the International Energy Agency (IEA), the fastest growing source of power in the world. Production of electricity from solar PV increased from 4 TWh in 1973 to 247 TWh in 2015 (IEA, 2017). Solar PV is solely dependent on insolation and has a long lifespan, in addition to decreasing in price and increasing in efficiency. However, large installations of PV power plants require vast land areas. Such land might be limited, due to high population density or scarcity.

Approximately 75 % of the world’s surface consists of water (Graham et al., 2010). By installing PV technology on water bodies, the potential for solar PV increases drastically. Floating PV (FPV) can be installed on inland water bodies and oceans, and is a technology in rapid growth.

Floating PV makes electricity more accessible. As several big and vastly populated cities are located by the shores, floating PV present as a viable solution, reducing the need for long transmission lines. FPV is also a viable solution for (desolated) islands and smaller communities by the shores. For the aquaculture industry, FPV can substitute the diesel generators, reducing noise and fuel costs, all the while producing clean electricity. Furthermore, FPV is generally capable of producing more electricity than a terrestrial installation of the same installed nominal power, due to lower operational temperatures caused by water cooling.

Previous research on FPV indicates that PV modules get cooled when being installed on pontoons, with a tilt. Thus, investigating the cooling effect for FPV installed horizontally, in thermal contact with water, is of interest.

1.2 Objective

The main objective of this work is to conduct and analyze an experiment at IFE, aimed at quantifying the cooling effect for a floating PV module in thermal contact with water. The difference in performance and module temperature between the floating module and a reference module is also central for the thesis. A thermal model has been developed to estimate the cooling effect and behavior of a floating module. Furthermore, two simulation software programs' abilities to simulate FPV are evaluated, based on the experimental results.

The work aims to cover the following:

- Establish a review of some studies on operational module temperature and efficiencies for FPV compared to terrestrial PV
- Describe the advantages and disadvantages with FPV
- Establish a test site and conduct an experiment on FPV module temperature and performance
- Develop a one-dimensional thermal model estimating the behavior of FPV
- Simulate FPV in software programs (PVsyst and TRNSYS), and evaluate their ability to correctly simulate FPV

The main objective was initially to analyze an experiment conducted by Ocean Sun, located in Singapore. The experimental setup would include Ocean Sun's actual concept; their canvas and materials, and would represent their technology. As this proved to be impossible within the timeframe of the thesis, it was decided to conduct a small-scale, but somewhat similar, experiment at IFE. The results might not be entirely applicable to Ocean Sun's concept, but give an indication on what might be expected from the technology.

2 Theory

The theory in chapters 2.1 – 2.4 relies on *Solar Energy - The physics and engineering of photovoltaic conversion technologies and system* (Smets et al., 2016) and *PVEducation.org* (Honsberg & Bowden, 2013). Theory from other sources are specified in each subchapter.

2.1 The sun

The sun is a sphere of gas with nuclear fusion reactions in the core, that convert hydrogen to helium. The reaction emits a lot of energy in terms of radiation. The total power due to the nuclear fusion is about 3.8×10^{26} W. Due to the distance between the Sun and the Earth, only about 1361 W/m^2 reaches the Earth's atmosphere. This is called the *solar constant*, which is an average value.

The solar constant varies slightly since the earth-sun distance changes as the earth moves in an elliptical orbit around the sun, and because the emitted power from the sun varies. The solar irradiation incident at the earth's surface varies substantially more. This is due to atmospheric effects such as absorption and scattering, local variations in the atmosphere such as water vapor, clouds and pollution, latitude of the location, the season of the year and the time of the day. Thus, the intensity, spectral content of the light and the angle from which the light is incident on a surface varies.

The light that we see is a fraction of the total incident irradiation. Light shows the behavior of particles, as well as waves. This behavior is called the wave-particle duality. "Packets" or quantas of energy are called photons. According to Planck's law, the photon energy is proportional to the frequency of the light:

$$E_{ph} = h\nu \quad (1)$$

where E_{ph} is the energy of the photon, h is Planck's constant and ν is the frequency.

2.1.1 Air Mass and angle of incidence

As discussed, the incident sunlight is affected by atmospheric effects, which reduces the amount that reaches a surface on earth. The Air Mass (AM) quantifies this reduction. The Air Mass is the path length for the incident light through the atmosphere divided by the shortest possible path length; when the sun is at zenith:

$$AM = \frac{1}{\cos(\theta)} \quad (2)$$

where θ is the angle from the zenith. When the sun is directly overhead, the Air Mass is 1.

In the summer months, the angle from zenith is generally lower than in the winter months, meaning that the light intensity is higher during summer. For the winter months, with lower solar altitude angles, α , the sunlight must traverse a longer path, as explained by the air mass ratio. This is illustrated in Figure 2.1.

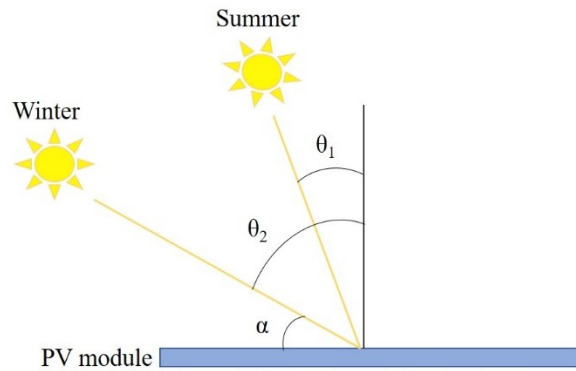


Figure 2.1: The path sunlight has got to traverse to reach a surface varies with season. The path is shortest when the sun is at zenith (directly overhead). The sun is closest to zenith during summer (θ_1), while further away during winter (θ_2). For a horizontal plate, the angle from zenith also represents the angle of incidence. α is the solar altitude angle, explaining the height of the sun relative to the ground.

2.1.2 Solar irradiance and solar insolation

The solar irradiance is an instantaneous power density in units of W/m^2 , which is strongly dependent on location and local weather, as discussed. Global horizontal irradiance is the total irradiance measured by a horizontal surface. The irradiance is usually divided into diffuse sunlight, caused by scattering, and direct sunlight.

The solar insolation (or irradiation) is the total amount of solar energy received at a specific location during a specified period, often in units of $\text{kWh}/\text{m}^2/\text{day}$ or $\text{kWh}/\text{m}^2/\text{month}$.

2.1.3 Albedo effect

The albedo coefficient is the fraction of global incident irradiation reflected by the surface in front of a PV module. The albedo will have no effect for a PV placed horizontally, but for tilted planes the effect increases as the tilt increases. The albedo varies according to season and surface. For an urban environment and grass surfaces, the albedo is around 0.2, while it is even lower for a water plane (PVsyst SA, 2017).

2.2 Angles for PV-installations

The tilt angle explains the module's tilt with respect to the horizontal. Thus, for a module placed horizontally, the tilt angle is zero. The orientation angle is used to describe the module's orientation with respect to the azimuth; the angle between the South vector and the module's normal vector on the horizontal plane. The orientation angle is of no importance for a horizontal PV module, but very important for tilted modules. The orientation angle for a tilted module faced towards the South is 0° .

The angle of incidence is the angle between the module's normal and the incident sunlight. For a horizontal module, the angle of incidence is equal to the angle from zenith, θ , as illustrated in Figure 2.1.

2.3 Photovoltaic theory

2.3.1 Generation of electricity

The process in which sunlight is converted directly into electricity using solar cells is called the photovoltaic effect. The photovoltaic effect is the generation of a potential difference at the junction of two materials in response to incoming solar irradiance.

The first part of the process leading to the photovoltaic effect is the generation of charge carriers in the solar cell materials due to absorption of light (photons). In an ideal semiconductor, electrons can have energy levels in the *valence band* or in the *conduction band*. The energy difference between the two allowed states is called the band gap:

$$E_g = E_C - E_V \quad (3)$$

If the energy of the photon equals the band gap, the electron can be excited from the valence band to the conduction band, leaving behind a “hole”. This hole causes a covalent bond to move from one electron to another, making it look like a positive charge. This process is illustrated in Figure 2.2. If the energy is below the band gap, the photon will traverse the material. However, if the energy exceeds the band gap, the electron will be excited and the excess energy will contribute to heating the material.

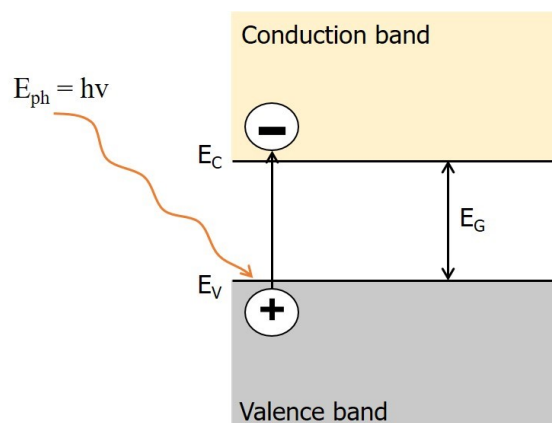


Figure 2.2: Illustration of the band gap of a semiconductor. Incoming photons must have energies higher than the band gap to excite an electron from the valence band to the conduction band.

Solar cells usually consist of a positive and a negative doped semiconductor material. The semiconductor material is often silicon, from group IV in the periodic table. Doping is a technique in which atoms from group III (boron) and group V (phosphorous) is added to the semiconductor, creating p-type and n-type materials, respectively. Atoms from group V has one more valence electron than silicon, while atoms from group III has one less valence electron. Only four valence electrons are needed from each atom to create covalent bonds around the silicon atom. Thus, in the n-type material, “free” electrons can participate in conduction. In the p-type material, not enough electrons are present to create covalent bonds, creating “holes”. Both materials are electrically neutral. These materials form a pn-junction. The “free” electrons at the boarder of the n-type diffuse towards the holes in the p-type, leaving behind a positive charged area and creating an internal electric field, called the depletion region. This is intended to separate electron-hole pairs and avoid recombination.

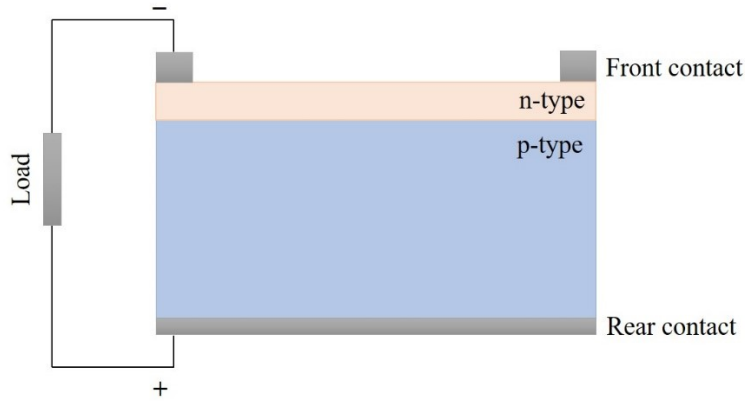


Figure 2.3: Illustration of the solar cell with its pn-junction and an external load. Under illumination, electrons will exit the solar cell at the front contact and generate a current, before recombining at the rear contact.

If the solar cell is an open circuit and under illumination, the numbers of electrons in the n-type and holes in the p-type will increase, as the electric field in the depletion region makes the electrons flow to the n-type material and the holes flow to the p-type material. The separation of positive and negative charges across the pn-junction is called a potential difference, which reduces the net electric field, and in turn leads to a diffusion current. The diffusion current is generated to balance out the surplus of carriers in the two materials. For the open circuit, an equilibrium is reached when the light generated current is balanced out by the diffusion current. The voltage over the pn-junction is then called the *open-circuit voltage*, V_{OC} . This is the maximum voltage available for a solar cell.

If the solar cell is connected to an external load, as illustrated in Figure 2.3, the charge carriers will exit the solar cell, generating a current. This happens because of the potential difference in the solar cell. If the solar cell is short-circuited, the carriers exit the solar cell and recombine as soon as they are generated, which means that there is no build-up of potential difference. The current is called *short-circuit current*, I_{SC} . For an ideal and unrealistic solar cell, the short-circuit current is identical to the light generated current. The short-circuit current is the largest current which can be drawn from the solar cell.

2.3.2 Solar cell parameters

Some parameters are often used to characterize the performance of PV modules.

- Short circuit current
- Open circuit voltage
- Maximum power point (MPP)
- Fill factor, FF
- Reference efficiency
- Nominal Operating Cell Temperature (NOCT)

The generated power from a PV module is the product of the current and the voltage. I_{MPP} and V_{MPP} gives the highest possible power output from a solar cell, P_{max} . The fill factor is the ratio between the maximum power and the product of V_{OC} and I_{SC} , as illustrated in Figure 2.4 and by the following equation:

$$FF = \frac{I_{MPP}V_{MPP}}{I_{SC}V_{OC}} \quad (4)$$

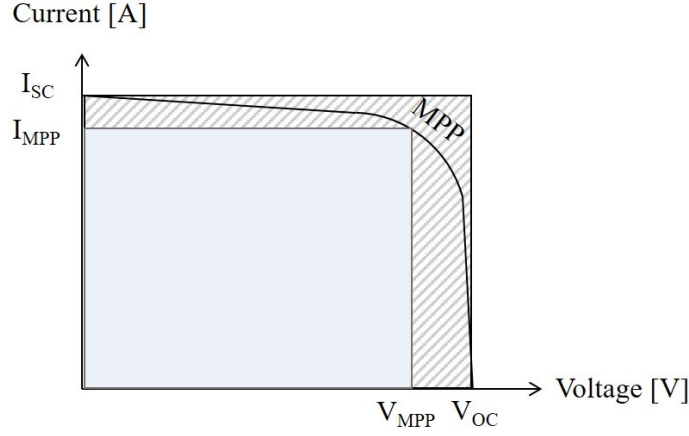


Figure 2.4: A sketch of an IV-curve, with short-circuit current, maximum power point current, open circuit voltage, maximum power point voltage illustrated and maximum power point. The fill factor is the ratio between the light blue area and the gray hatched area.

The efficiency of the solar cell is the ratio between maximum power output, P_{max} , and the incident solar irradiance on the module:

$$\eta = \frac{P_{max}}{P_{in}} = \frac{I_{MPP}V_{MPP}}{P_{in}} = \frac{I_{SC}V_{OC}FF}{P_{in}} \quad (5)$$

P_{max} and hence the efficiency also depends on the spectrum and intensity of the incident sunlight, and the temperature of the solar cell. At higher ambient temperatures, the cell and module temperature increase.

There are different equations and ways to determine the cell temperature of a module, when it is not directly measured. For uniform and one-dimensional conduction, the following equation may be used (Kratochvil et al., 2004):

$$T_c = T_m + \frac{I_L}{I_{L0}} \Delta T \quad (6)$$

where T_c is the cell temperature, T_m is measured back-surface module temperature, I_L is measured solar irradiance on the module surface and I_{L0} is the reference solar irradiance at 1000 W/m^2 . ΔT is given as 3°C for glass/cell/polymer sheet modules with open rack mounting (Kratochvil et al., 2004).

However, if the back-surface module temperature is unknown, the following equation may be used to estimate the cell temperature:

$$T_c = T_{amb} + \frac{NOCT - 20}{800} I_L \quad (7)$$

where T_{amb} is the ambient temperature and $NOCT$ is the nominal operating cell temperature. The $NOCT$ is usually provided by the manufacturer, and is defined under the following conditions; irradiance at 800 W/m^2 , air temperature at 20°C , wind speed at 1 m/s and open rack mounting.

2.3.3 The two-diode model

The behavior of a solar cell can be described by the equivalent circuit. The single-diode model is a circuit with a diode and a current source connected in parallel, in which the diode represents the pn-junction. For an ideal solar cell, there will be no internal losses. However, a non-ideal solar cell will have losses related to recombination of the electron-hole pairs. To model this more accurately, two

diodes can represent the pn-junction, in a two-diode model, in which one is ideal and one is non-ideal. This is described with an ideality factor equal to one or greater than one, respectively. The equivalent circuit for the two-diode model is illustrated in Figure 2.5. The relation between the current and the voltage is given by the following equation:

$$I = I_{ph} - I_{d1} - I_{d2} - I_p = I_{ph} - I_{01} \left\{ \exp \left[\frac{q(V+IR_S)}{n_1 k_B T} \right] - 1 \right\} - I_{02} \left\{ \exp \left[\frac{q(V+IR_S)}{n_2 k_B T} \right] - 1 \right\} - \frac{V+IR_S}{R_P} \quad (8)$$

where T is the cell temperature in Kelvin, n_1 and n_2 are the ideality factors, k_B is the Boltzmann constant, q is the elementary charge, I_{01} and I_{02} are the saturation currents of the diodes, I_{d1} and I_{d2} are the currents through the diodes, I_p is the current through the shunt resistance, I_{ph} is the light generated current, R_S is the series resistance and R_P is the shunt resistance.

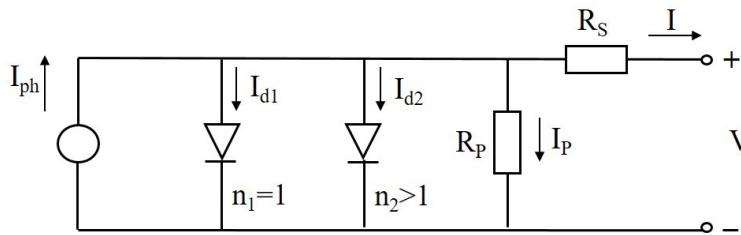


Figure 2.5: The equivalent circuit illustrated by the two-diode model. n_1 and n_2 are the ideality factors, I_{d1} and I_{d2} are the currents through the diodes, I_p is the current through the shunt resistance, I_{ph} is the light generated current, R_S is the series resistance and R_P is the shunt resistance.

The series resistance, R_S , is the sum of the resistance in the semiconductor material, the contact resistance between the metal contact and the silicon in the semiconductor and the resistance of the top and rear metal contacts. It affects the current and the fill factor of the solar cell.

The shunt resistance, R_P , occurs due to manufacturing defects, providing an alternate current path for the light-generated current. This reduces the current through the pn-junction, which in turn reduces the voltage.

2.3.4 Solar cell efficiency

As discussed in subchapter 2.3.2, the solar cell efficiency is affected by the cell temperature, the light intensity and the angle of incidence.

2.3.4.1 Measurements of efficiency

Solar cells and PV modules are tested under standard test conditions (STC) to fairly compare them under the same conditions. The test conditions are defined at irradiance of 1000 W/m^2 , a cell temperature at $25 \text{ }^\circ\text{C}$ and AM1.5 spectrum.

Flash testing is also often used to test the parameters of the solar modules, in which light is flashed on the cell and measurements are taken very quickly. This eliminates temperature control problems.

Tests like these give all the parameters listed in subchapter 2.3.2, and create an IV-curve as illustrated in Figure 2.4.

2.3.4.2 Temperature dependent efficiency

The operating temperature of a PV module has great impact on its performance, as previously discussed. By decreasing the operational temperature, the efficiency is most likely to increase (Dash & Gupta, 2015; Liu et al., 2017).

In a semiconductor, an increase in temperature will increase the energy of the electrons, thus reducing the band gap. Now, less energy is needed to excite electrons to the conduction band. Both the open circuit voltage and the fill factor decrease substantially with temperature, as the thermally excited electrons begin to dominate the electrical properties of the semiconductor. Since electrons will more easily be excited, the carrier concentration will increase, leading to higher diffusion current and lower open-circuit voltage. The short-circuit current will increase slightly due to the increased carrier concentration, but not enough to compensate for the reduction in V_{OC} . The net effect leads to a linear relationship (Skoplaki & Palyvos, 2009):

$$\eta = \eta_{STC} [1 - \beta(T_c - T_{STC})] \quad (9)$$

where η_{STC} is the module's efficiency at the reference temperature, T_{STC} , and at solar irradiance of 1000 W/m^2 . The efficiency is usually provided in the datasheet, and the reference temperature is 25°C . β is the temperature coefficient of P_{MPP} , which is material specific and usually provided by the manufacturer in the PV module's datasheet. The temperature coefficients of V_{OC} and I_{SC} are usually also provided.

The power output from a PV module will also be temperature dependent, and it may be described as a function of the temperature dependent efficiency (Skoplaki & Palyvos, 2009):

$$P = I_L \eta_{STC} A [1 - \beta(T_c - T_{STC})] \quad (10)$$

where I_L is incoming irradiance and A is the surface area of the module.

2.3.4.3 Effect of light intensity and angle of incidence

The light intensity affects the short-circuit current, the open circuit voltage, the fill factor, the efficiency and the internal resistances.

The shunt resistance affects the solar cell at low light intensities, as the current through the solar cell is low and more passes through the resistance, causing losses. At high light intensities, the series resistance has a greater impact on losses due to higher currents.

PV modules perform best when the incident light is normal to the module surface. At higher angle of incidence, typically beyond 55° , the reflectance on the glass surface of the modules increases, reducing the ability to absorb irradiation (Kratochvil et al., 2004).

2.3.5 Solar cell technologies

There exists a range of different solar cell technologies. This thesis focuses on crystalline silicon (c-Si) semiconductors, which is the dominating technology. There are two different types of c-Si; monocrystalline and multicrystalline.

Monocrystalline usually have improved material parameters than multicrystalline, but they are more expensive. The monocrystalline structure is ordered with each atom ideally placed in a pre-determined position, while the multicrystalline structure is more random with grain boundaries.

2.3.6 Performance ratio

The performance ratio (PR) is the ratio of produced power over power produced at STC. It is independent of orientation and incident irradiance, and can thus be used to compare installations at different locations:

$$PR = \frac{P_{measured}}{P_{STC}} \quad (11)$$

The PR is affected by parameters such as mechanical losses, soiling, temperature effects, reflection and shading. It is not possible to reach 100 % due to unavoidable losses, but good designs can reach a PR of approximately 85 %.

2.4 Heat transfer

This subchapter of the theory relies much on Bergman et al. (2011) in addition to the already specified sources. Other sources are specified in the text.

A PV module exposed to sunlight converts approximately 10-20 % of the incoming sunlight to electricity. The rest of the energy is converted into heat. Heat is generated by the photovoltaic activities in the cells and by the emitted radiation at the infrared wavelength of the solar spectrum (Armstrong & Hurley, 2010).

How much of the incoming sunlight that contributes to heating of the modules depend on several factors, such as the reflection from the top surface of the module, the electrical operating point of the module, absorption of sunlight by the regions not covered with solar cells, absorption of low energy light in the module and the packing density of the solar cells.

The solar irradiance absorbed by PV modules must be equal to the power produced and overall heat flux in the modules. Thus, the heat flux, Q , may be defined as:

$$Q = I_L \times A - \eta I_L \times A = I_L(1 - \eta) \times A \quad (12)$$

where I_L is the incident irradiance on the surface and A is the surface area of the module. As a horizontal installation of PV modules is most relevant for the work in this thesis, the incident irradiance on the modules will equal the *global horizontal irradiance*, G_{hor} .

The amount of solar irradiation absorbed by the solar cells depend on the material specific absorption coefficient, which is generally equal to 0.9. It is assumed that this coefficient is underlying in the electrical efficiency, η .

The overall heat loss in a PV module is the sum of several heat transfer mechanisms; convection, conduction and radiation, as illustrated in Figure 2.6.

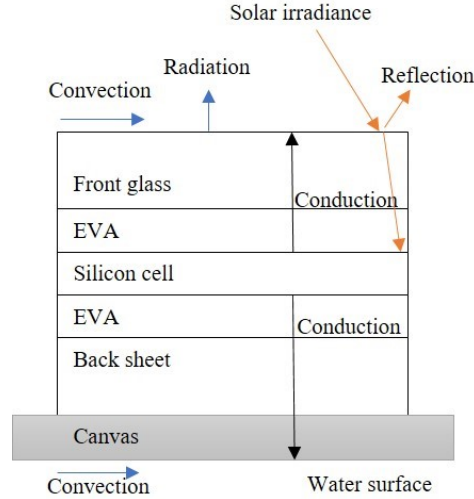


Figure 2.6: Configuration of a PV module and illustration of heat loss mechanisms. For this thesis, the module is depicted on a water surface, to illustrate the convection caused by the water surface.

2.4.1 Thermal loss factor

The thermal loss factor, *the U-value*, indicates the effectiveness of module cooling by the environment (Reindl, 2018). It can be calculated from measured ambient temperature, wind speed, surface irradiance and module temperature. The higher the *U-value*, the lower the operational cell temperature and hence the higher efficiency.

The U-value consists of two parts (PVsyst SA, 2018):

$$U = U_c + U_v \times v \quad (13)$$

where U_c is the constant loss factor, U_v is the variable wind loss factor and v is the wind speed. At higher wind velocities, the thermal loss will generally increase.

A common U-value for a roof-top PV system is 20-30 W/m²K, while it for floating systems have been measured to approximately 40-60 W/m²K (Reindl, 2018). Greene et al. (2016) suggests a U-value for an installation in thermal contact with water of approximately 65 W/m²K.

The U-value is defined as the excess heat from the irradiance divided by the temperature difference between the solar cell and the ambient (PVsyst SA, 2018):

$$U = \frac{G_{hor}(1 - \eta)}{T_c - T_{amb}} \quad (14)$$

It may also be expressed by other parameters, by adjusting it for the wind velocity (TRNSYS Technical Support Team, 2018):

$$U = \frac{I_{NOCT} \tau \alpha}{T_{c,NOCT} - T_{amb,NOCT}} \times \frac{5.7 + 3.8v}{9.5} \quad (15)$$

This expression relies on several given parameters, provided in the PV module's datasheet, and for each module the definition may be written on the form as equation 13. $\tau \alpha$ usually has a default value of 0.95 (TRNSYS Technical Support Team, 2018)

2.4.2 Convection

Convective heat transfer is a mechanism that occurs due to transportation of heat away from a surface, as the result of a fluid moving across the surface of another. The transferred heat in this process is given by Newton's law of cooling:

$$Q = hA\Delta T = \frac{\Delta T}{R} \quad (16)$$

where h is the convection heat transfer coefficient, A is the contact area for the two materials in and ΔT is the temperature difference between the two materials. R is the thermal resistance, given as:

$$R = \frac{1}{hA} \quad (17)$$

There are two ways for heat convection to occur; either by natural (free) convection or by forced convection. If the motion of the fluid arises from an external agent, such as a fan or the wind, the process is called forced convection (Bejan & Kraus, 2003). The process is called natural or free convection when there is little or no wind present, and the motion is caused by density differences, for instance.

The convective heat transfer coefficient is complex and often determined experientially. The *forced convection coefficient*, h , for a horizontal flat plate with laminar flow is given by the following equations (Bejan & Kraus, 2003):

$$h = \frac{Nu \times k}{L} \quad (18a)$$

$$Nu = 0.664 Re^{1/2} Pr^{1/3} \text{ for } Pr \geq 0.7 \quad (18b)$$

$$Re = \frac{\rho v_k L}{\mu} \quad (18c)$$

where Nu is the Nusselt number, k is the thermal conductivity, L is the thickness of the material, Re is the Reynold number, Pr is the Prandlt number, ρ is the density, v_k is the kinematic viscosity and μ is the dynamic viscosity of the fluid.

The *natural convection coefficient* for a horizontal flat plate with laminar flow is given as:

$$h = \frac{Nu \times k}{L} \quad (19a)$$

$$Nu = 0.52 Ra^{1/5} \quad \text{for } 10^4 \leq Ra \leq 10^9, Pr \geq 0.7 \quad (19b)$$

$$Ra = Gr \times Pr \quad (19c)$$

$$Gr = \frac{g\beta_{th}(T_s - T_\infty)L^3}{\nu^2} \quad (19d)$$

where Ra is the Rayleigh number, Gr is the Grashof number, g is the gravity constant, β_{th} is the coefficient of thermal expansion, T_s is the surface temperature and T_∞ is the bulk temperature.

The Nusselt number provides a ratio of convection to pure conduction heat transfer. The Reynold number is the ratio of inertia to viscous forces in a region of length L . The Prandtl number is the ratio of momentum diffusivity to thermal diffusivity. If the Rayleigh number is below a critical value for a fluid, heat transfer is primarily in the form of conduction, and if it exceeds the critical value, heat transfer is primarily in the form of convection. Grashof number is a measure of the ratio of buoyancy forces to

viscous forces. Errors as large as 25 % may be incurred by using these expressions, due to uncertainties related to each equation and parameter.

2.4.3 Conduction

Conductive heat loss in an object is due to thermal gradients between the object and other materials. The ability to transfer heat to surroundings is characterized by the thermal resistance and the configuration of the object. The heat transferred in the process is given by Fourier's law:

$$Q = -kA \frac{dT}{dx} = kA \frac{\Delta T}{L} = \frac{\Delta T}{R} \quad (20)$$

where k is the thermal conductivity, A is the surface area, L is the material thickness, ΔT is the temperature difference between the gradients, assuming a linear relationship. R is the thermal conductive resistance:

$$R = \frac{L}{kA} \quad (21)$$

2.4.4 Radiation

Radiation is heat transfer to the surrounding environment from an object. Any object will emit radiation based on its temperature, depending on its emissivity. A PV module is a non-ideal blackbody. The net radiative loss is the difference between the heat emitted from the surroundings to the module and the heat emitted from the module to the surroundings. For a horizontal module, only the top surface and sides will emit radiation. The radiation from the sides is negligible due to the very small surface area. The radiation is defined as:

$$Q_{rad} = \varepsilon F \sigma A (T_m^4 - T_{amb}^4) \quad (22)$$

where ε is the emissivity of the surface, F is the view factor and σ is Stefan-Boltzmann constant.

2.5 Floating PV

Photovoltaics installed at rooftops and ground-mounted installations is the norm. However, the interest of installing PV on water surfaces have grown rapidly the last years, and countries such as Japan, South Korea, the UK, China and India already have several installations of floating PV (Reindl, 2018).

Floating PV can be installed on different water bodies, both inland and on the open sea. There are several advantages and reasons for installing PV on water bodies:

- Valuable land is conserved, such as agricultural land. This is optimal for regions with scarce land resources, but available water bodies.
- Water will be conserved, as the modules prevent water evaporation. It also limits algae growth and potentially improves water quality (Sahu et al., 2016).
- There will be less shading on the modules due open and flat surfaces.
- Lower cell temperature and higher efficiency, caused by the evaporative effect of water.
- Less dust accumulation on the modules. Especially for installations on larger water bodies where the wind velocity will be higher and the distance to land greater.

- Potential of integration with aquaculture.
- Potential of integration with hydropower stations due to the already existing infrastructure and potential benefits of hybridization, ensuring stable power production.
- Reduction of transmission costs due to available water bodies close to densely populated areas.

Disadvantages:

- Investment costs are likely to be higher than conventional solar plants (Sahu et al., 2016).
- Higher risk of damages caused by high tides, waves, storms, cyclones and tsunamis. This is highly dependent on the location and the region of the installation.
- Possibly shorter life time due to increased corrosion and high moisture content because of proximity to (salt) water.
- Potentially a negative effect on fish and algae growth.
- Fishing and recreational activities, if any, is likely to be affected.
- Shellfish attaching to the installations might cause unwanted effects, such as less heat transfer through the bottom surface.

2.5.1 Operational temperature of floating PV

For floating PV installations, the evaporative effect of water cools the bottom of the modules, decreasing the operational temperature (Choi, 2014; Sahu et al., 2016). For a test site in Singapore, there is an installation with active water cooling which has shown even lower operational temperatures than the other installations (Reindl, 2018).

There are several ways to decrease the module temperature. Active water cooling has proven to give a reduction in the module temperature and an increase in the efficiency (Bahaidarah et al., 2013; Liu et al., 2017). Thus, for installations in thermal contact with water, there is reason to believe that the efficiency will be significantly increased (Azmi et al., 2013; Trapani & Millar, 2014).

Table 2.1: Review of some studies on module temperature and efficiencies for floating solar PV compared to terrestrial PV

Author	Decrease in module temperature	Increase in efficiency
Choi (2014)	Not specified	11 %
Liu et al. (2017)	3.5 °C	1.58 – 2 %
Azmi et al. (2013)	3.5 °C	2.82 – 14.58 %
Trapani and Millar (2014)	8 °C	5 %

2.5.2 Costs of floating PV

The costs of a floating PV installation will depend on many factors, predominantly related to the choice of components and materials, and the of water body for the installation. Thus, it is very hard to estimate the costs of a floating plant, unless every aspect of it is known. Cost estimates will have a high degree of uncertainty.

The costs for a floating system can be about 30 % higher than a conventional grid-connected installation, with the floating structure accounting for 20-30 % and the PV modules for 40 % of the total CAPEX (Ferrer-Gisbert et al., 2013). Nevertheless, the module-cost is decreasing each year.

It is likely that operation and maintenance (O&M) costs will be lower than for terrestrial PV installations, as components are less likely to overheat, and soiling and bird dropping is likely to be reduced (Sahu et al., 2016). For an installation at sea, it is likely that waves will wash the modules and thus reduce the need for human cleaning. However, there is a lot of uncertainty with respect to the possible degradation due to seawater and the possible accumulation of salt on the surface of the modules. Such effects might lead to higher O&M costs.

There will be little costs related to preparing the installation area, but there will be costs related to the mooring system. For an off-shore installation connected to the grid, underwater cables will be a necessity. Multiconsult suggests approximately 8 MNOK/km of cables (Greene et al., 2016).

The levelized cost of electricity may be used to compare different installations. It is the price at which electricity must be generated from a specific source to break even over the lifetime of the project. It is an economic assessment of the cost of the energy-generating system including all costs over its lifetime (Afework et al., 2018):

$$LCOE = \frac{\sum_{t=1}^n \frac{I_t + M_t + F_t}{(1+r)^t}}{\sum_{t=1}^n \frac{E_t}{(1+r)^t}} \quad (23)$$

where I_t is the investment expenditures, M_t is the O&M expenditures, F_t is the fuel expenditures, E_t is the electricity generation, t is the year, r is the discount rate and n is the lifetime of the system.

2.5.3 Current installations

Most installations today consist of a pontoon, with arrays of PV modules, moored to the ground. There has been a rapid growth in the floating solar PV plants the last decade, and the growth is not assumed to stop any time soon (Liu et al., 2017; Sahu et al., 2016). For the top 70 plants, the cumulative capacity has more than doubled in comparison with the previous year (Mesbahi & Minamino, 2018). However, such installations are predominantly installed in inland water bodies, and not the open sea.

Table 2.2: Top 10 floating solar plants worldwide (Mesbahi & Minamino, 2018)

Rank	Size (MW)	Name	Country	Company name	Water body
1	40	Coal mining subsidence area of Huainan City	China	-	Artificial lake
2	20	Coal mining subsidence area of Huainan City	China	-	Artificial lake
3	9.982	Pei County	China	Ciel & Terre	Inland
4	7.550	Umenoki	Japan	Ciel & Terre	Inland
5	6.776	Jining GCL	China	Ciel & Terre	Inland
6	6.338	Queen Elizabeth II Reservoir	UK	Ciel & Terre	Reservoir
7	3	Cheongpung Lake	South-Korea	LG CNS	Lake
8	3	Otae Province	South Korea	LG CNS	Reservoir
9	3	Jipyong Province	South Korea	LG CNS	Reservoir
10	2.991	Godley Reservoir Floating Solar PV	UK	Ciel & Terre	Reservoir

Of the 70 largest floating solar power plants, 54 are in Japan, making Japan the leading country on this technology. The majority of these are located on dams. South Korea is the second leading country followed by China, the UK, Taiwan and Belgium (Mesbahi & Minamino, 2018).



Figure 2.7: Floating solar power plant in Huainan, China (Brandon, 2017)

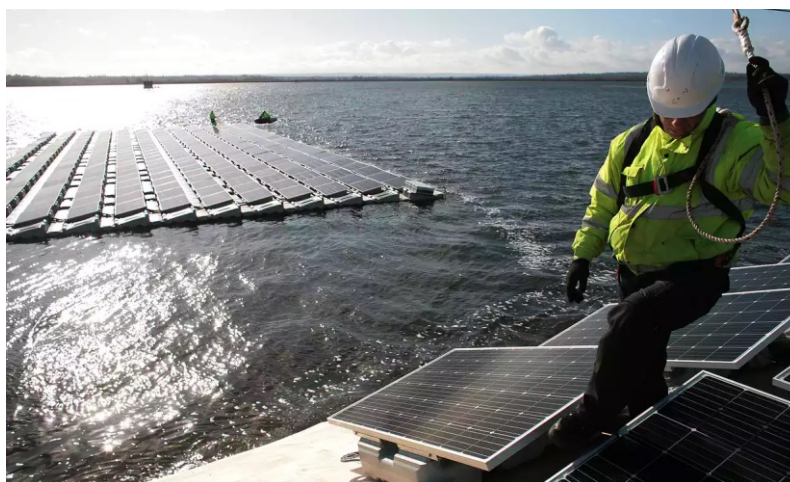


Figure 2.8: Queen Elizabeth II reservoir solar farm (Harvey, 2016)

In addition to the plants described above, there is a test bed of floating PV located on an inland water body in Singapore, consisting of ten installations by different manufacturers and companies (Reindl, 2018). The testbed aims to study the technical, economic and environmental feasibility of large-scale floating PV systems.



Figure 2.9: Testbed in Singapore with 10 installations of floating PV (Reindl, 2018)

While floating PV plants on inland water bodies are emerging at high speed, the installations at sea are still waiting to emerge. Swimsol was the first at implementing floating solar PV at sea. There are several projects aimed at installing off shore floating PV plants (Bellini, 2018). Ocean Sun has a prototype placed at the Norwegian west coast (Løvik, 2017).

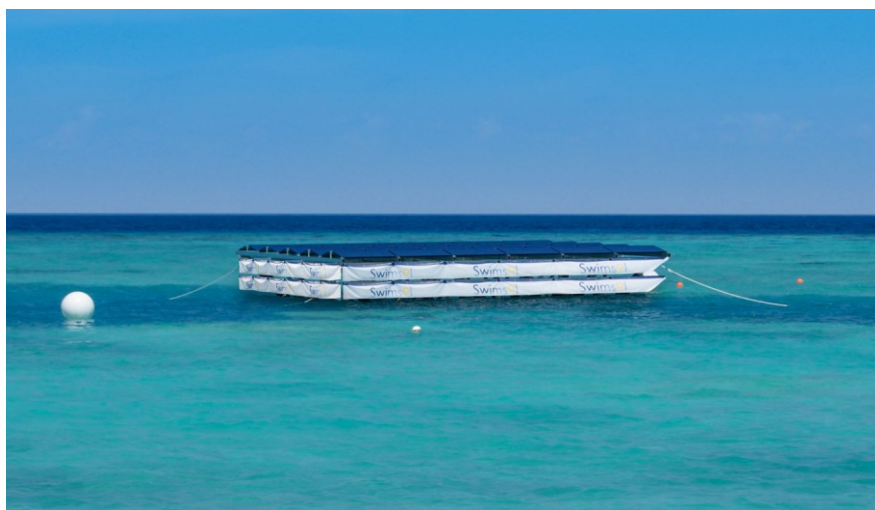


Figure 2.10 (Swinsol, by permission): Swimsol's installation in the Maldives - the first installation at sea.



Figure 2.11 (Ocean Sun, by permission): Ocean Sun's prototype situated at the West coast of Norway.

2.5.4 Ocean Sun's concept

Ocean Sun is a start-up company based in Norway working on a solution for floating PV for offshore installations. The technology is based on horizontal PV modules on a floating structure. The PV modules are modified to achieve low operating cell temperatures through direct heat transfer with water. The floating structure is designed to withstand waves and typical offshore conditions (Ocean Sun, 2017).

The technology is under continuous development to improve the solution, in terms of the support structure, PV module technology, module temperature and annual yield.

3 Method

The first part of this chapter describes the test stations for the experiments conducted at IFE and in Singapore. Then the analytical methodology used to analyze the experimental data obtained from the test site at Kjeller is described. Next, the mathematical model is described, aiming to model the experimental site at Kjeller and the cooling effect. Lastly, the computer modeling is described, aiming to simulate the experimental results.

3.1 Test station: IFE, Kjeller

3.1.1 Layout and surroundings

The test station is located at the Institute for Energy Technology (IFE) at Kjeller, Norway, with latitude 59.973180 and longitude 11.051269.

The setup consisted of two 270W REC Peak Energy modules (multicrystalline silicon) outside the Solar Building, as illustrated in Figure 3.1. The module lying on the grass is hereby called the *reference module*, while the module lying on the inflatable pool is called the *floating module*.

The reference module was placed on wooden lists, lifting it from the grass and leading to some air circulation at the back side, in addition to ensuring that it was horizontal. The floating module was placed on a canvas (tarp) which was placed over the pool's surface. It had its frame removed to assure good thermal contact with the surface of the canvas and water. Both modules have the junction box and cables on the back side. This leads to some air gaps between the contact area for the floating module and the canvas.

There are several buildings and structures surrounding the experimental setup, such as a lamp post, a rack of 15 PV modules, two tables and a metal cylinder. In addition, there was snow surrounding the setup, which melted during the test period. The surrounding buildings protect the modules from wind. Due to the buildings, sunlight hits the surface of the reference module before hitting the floating module. There are no objects casting shade over the modules during the day.



Figure 3.1: The setup of the modules on the test site. The measuring equipment is connected to the grid. The reference cell and temperature sensor are at the PV rack to the right in the figure.



Figure 3.2: Left: Reference module lifted from the ground by wooden lists. Right: Floating module placed on the canvas. The frame is removed from the module.

3.1.2 Insolation and temperature at the test site

The average annual horizontal insolation at Kjeller is about 900 kWh/m^2 , which is approximately the average for Norway (JRC EC, 2017). This is based on the PVGIS-CM-SAF database. See Figure 3.3 for illustration.

The experiment was conducted in April, with an average temperature of approximately $5 \text{ }^\circ\text{C}$. Optimally, the experiment would have been conducted in June or July, when the average insolation and temperature is the highest. The average wind speed for the days in April in which the experiment was conducted was 2.35 m/s (*Været som var (detaljert) Kjeller Flyplass, Skedsmo (Akerhus), 2018*).

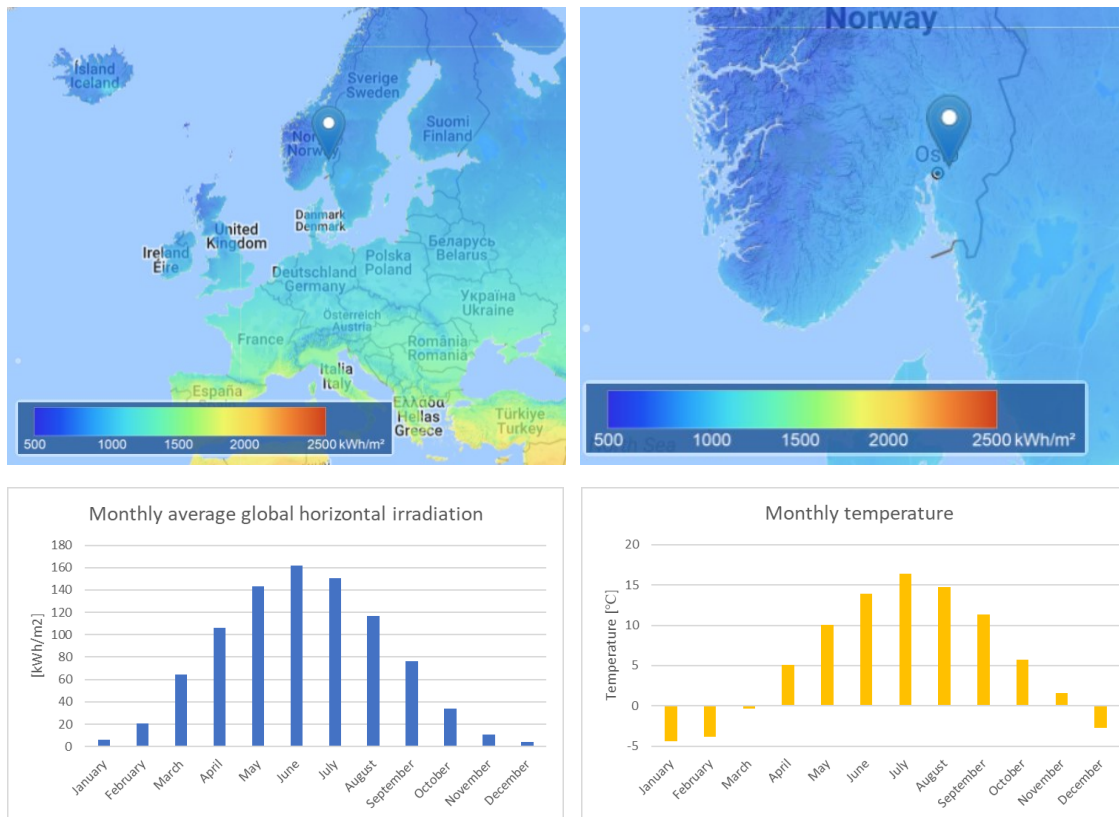


Figure 3.3: Top left: Map over average irradiation for parts of Europe (JRC EC, 2017). Top right: Average irradiation for parts of Norway. Kjeller is marked with the pin. Bottom left: Monthly average global horizontal irradiation at Kjeller, illustrating the seasonal differences. Bottom right: Monthly average air temperature at Kjeller.

3.1.3 Measurements at test station

Global horizontal irradiance and ambient temperature is measured at the PV rack close to the setup. Unfortunately, wind speed is not measured at the test site, but at Kjeller Airport, which is approximately 1 km away from the test site.

The modules are connected to the same microinverter, YC500I, from Altenergy Power Systems (APS) and the power output is logged every five minutes with an energy communication unit (ECU) from APS. The time stamp of the logging was not synchronized with the irradiance logging. The microinverter has a peak efficiency of 95.5 % (APSystems, 2016).

The microinverter is connected to a power outlet directly near it, and the modules are connected to the microinverter with an extension cord. Thus, the system losses are relatively small, and equal for the floating and the reference module.



Figure 3.4: Left: Microinverter from APS, type YC500E. Right: Energy communication unit from APS, ECU-3 V3.

3.1.3.1 Irradiance

The global horizontal irradiance is measured by a reference cell. The reference cell was calibrated June 1st, 2017. The reference cell is an Analog Silicon Irradiance Sensor, type Si-01 TC, from Ingenieurbüro Mencke & Tegtmeyer GmbH. A typical measurement uncertainty is 2 W/m², while the overall measurement uncertainty is $\pm 5\text{W/m}^2$ or $\pm 2.5\%$ of measurement value (Ingenieurbüro Mencke & Tegtmeyer GmbH, 2016).

The SolarEdge Control and Communication Gateway, SE1000-CCG-G logs the measurements with an accuracy of $\pm 1\%$ (SolarEdge Technologies, 2014). The logged value is the root mean square of the five-minute sampling.



Figure 3.5: The reference cell measuring global horizontal irradiance.

3.1.3.2 Ambient temperature

Ambient temperature is measured with the Ta-V-4090 ambient temperature sensor from Ingenieurbüro Mencke & Tegtmeyer GmbH. It is logged every five minutes. The uncertainty of the sensor is of 1 K (Ingenieurbüro Mencke & Tegtmeyer GmbH, 2018).

3.1.3.3 Back-surface module temperature

PT100 temperature sensors were connected to the back-surface of each module two times; Tuesday 10.04.18 and Thursday 12.04.18. The sensors could unfortunately not be connected at night time, as it was connected to a computer that had to be placed at the test site. The equipment was not suited to be outside at night due to night frost. For that reason, the sensors were disconnected and logging was stopped between 16.00 and 17.00. The sensors were resistance temperature detectors (RTD) and the accuracy was assumed to be of $\pm 1^\circ\text{C}$.

Each module had two sensors connected, as illustrated in the figure below. Tape was used to ensure contact between the sensor and the module surface. The tape unfortunately leads to lower heat transfer.

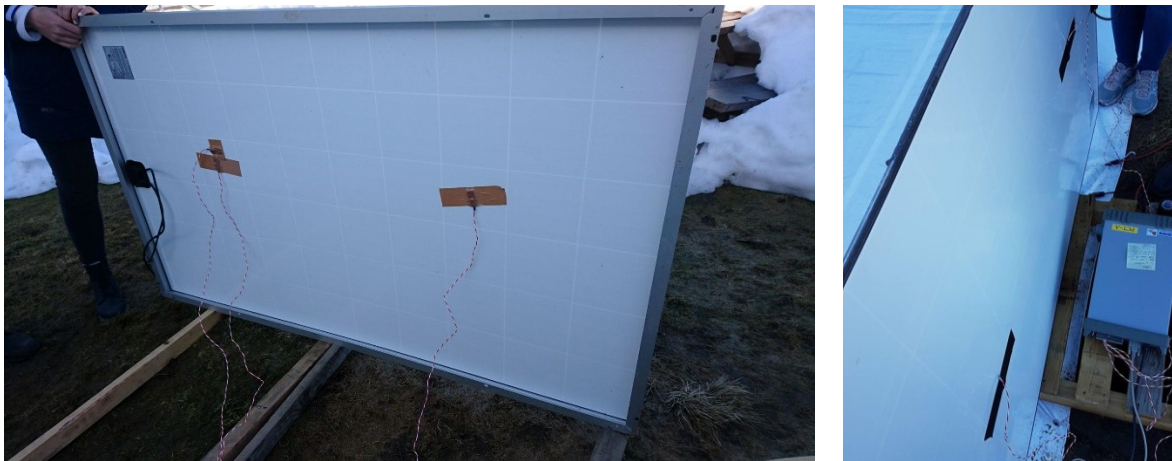


Figure 3.6: Left: Temperature sensors connected to the reference module, with tape (the top left one was tested because the aluminum was gone, and is not included in the analysis). Right: Temperature sensors on the floating module, connected with electrical tape.

3.1.3.4 Solar simulator

Both modules were flash tested by a solar simulator to find their individual IV-curve and maximum power point. This was done on Monday 09.04.18. The solar simulator is the Spi-Sun SimulatorTM 5100SLP Blue system from Spire.



Figure 3.7: Sun simulator from Spire used for flash testing both modules.

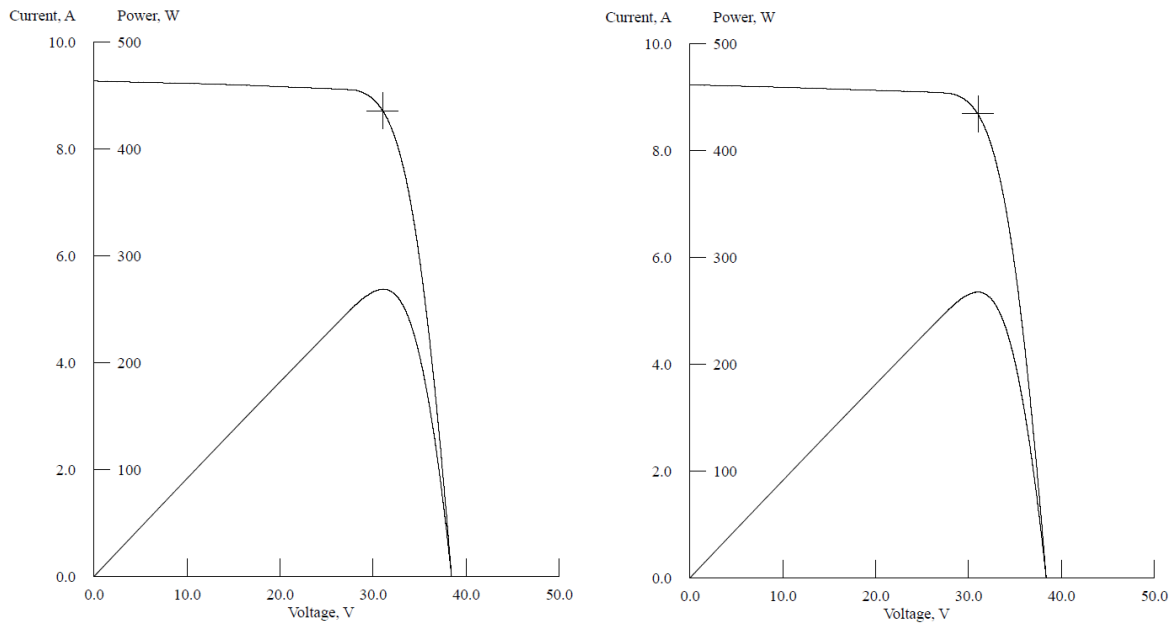


Figure 3.8: Left: The IV-curve for the reference module, $P_{max} = 268.8 \text{ W}$. Right: The IV-curve for the floating module, $P_{max} = 267.6 \text{ W}$

For the reference module, 3449 IV-pairs were logged in the flash test. 3583 IV-pairs were logged for the floating module. The uncertainty in the testing was checked with a repeatability test. The standard deviation divided by average value for I_{SC} , V_{OC} , P_{max} and FF were all less than 0.15.

Thus, for further analyses, the respective P_{max} values have been used in the calculations.

Table 3.1: Results from flash test by sun simulator, Monday 09.04.18.

	Reference module	Floating module
Serial number	4005652613	4005652604
Pmax [W]	268.8	267.6

3.1.3.5 IR pictures

Pictures were taken of the modules with an infrared camera, FLIR A325, on Tuesday 10.04.18. There were some challenges with taking good pictures of the modules, as there was much reflection from the surroundings. In addition, the temperature scale on the camera is not correct, showing lower values than measured with the back-surface temperature sensors.

A potential reason for the offset is that the camera was last calibrated January 23rd, 2009. The accuracy is stated to be $\pm 2^{\circ}\text{C}$ or $\pm 2\%$ of the reading, depending on which value is the largest (FLIR Systems, 2014). A new camera was purchased, but unfortunately not in time to be used for this work.

The software used for taking and analyzing the pictures is ThermaCAM Researcher Pro 2.9. Matplotlib in Python was used to plot the pictures and present them.

The detector type is an uncooled microbolometer, the spectral range is $7.5 - 13.0\ \mu\text{m}$ and the resolution is 320×240 .



Figure 3.9: IR camera used for mapping the surface temperatures of both modules

3.1.3.6 Water temperature

The water temperature was measured with a commercial Indoor & Outdoor Thermometer from CO/TECH. This was not calibrated and was not explicitly intended for water temperature measurements, but assumed to give approved estimates. The temperature was generally measured to approximately 4°C throughout the days. The uncertainty and accuracy for the instrument is unknown.



Figure 3.10: Instrument for measuring the water temperature in the pool. Picture taken 10.04.18 at 14.39. Note how the timestamp on the thermometer is incorrect.

3.2 Test station: Singapore

Initially, the idea for the thesis was to analyze an experiment conducted by Ocean Sun, situated in Singapore. However, due to some unforeseen technical and logistical issues, continuous logging of data was not possible to obtain by the timeframe for the thesis. The inverters used were off grid and offline. There were some issues related to batteries at the site, in which it broke during discharging, in addition to it charging too quickly. Thus, no data was collected or analyzed for the test site.

The test site in Singapore is still active and Ocean Sun is working on improving the solution to be able to obtain and analyze data.

3.2.1 Layout and surroundings

A floating canvas, of Ocean Sun's concept, placed on the water surface close to the shore, consists of 12 modules of 290W REC Twin Peak, as illustrated in Figure 3.11. To the left, six modules are placed in a string, lifted by wooden lists. This leads to air cooling and removes the modules from the water contact.

To the right, six modules are placed in a string directly onto the canvas. The original aluminum frames are removed. This leads to thermal contact with the canvas and water surface. However, as there are three junction boxes and cables at the back side of each module, local air gaps occur reducing the overall thermal contact.

For the string of laminates, an increase in effect by approximately 10 % has been measured, from direct readings, compared to the reference modules. According to Ocean Sun, the IR camera gives approximately 33°C for the water surface, 35°C for the laminate surfaces and 63°C for the lifted module surfaces. Such a difference in temperature suggests that the increase in effect should be 10.1 %, given a temperature coefficient for P_{MPP} equal to $-0.36 \text{ \%}/^{\circ}\text{C}$ and internally equal modules. This coincides well with the preliminary results. The IR pictures shows clear signs that the junction boxes and cables locally increase the module temperature.

Figure 3.12 clearly shows a difference in module temperature.



Figure 3.11 (Ocean Sun, by permission): Top: Experimental setup of 12 modules in Singapore. Bottom left: Reference modules lifted by wooden lists. Bottom right: Laminates in thermal contact with the canvas.

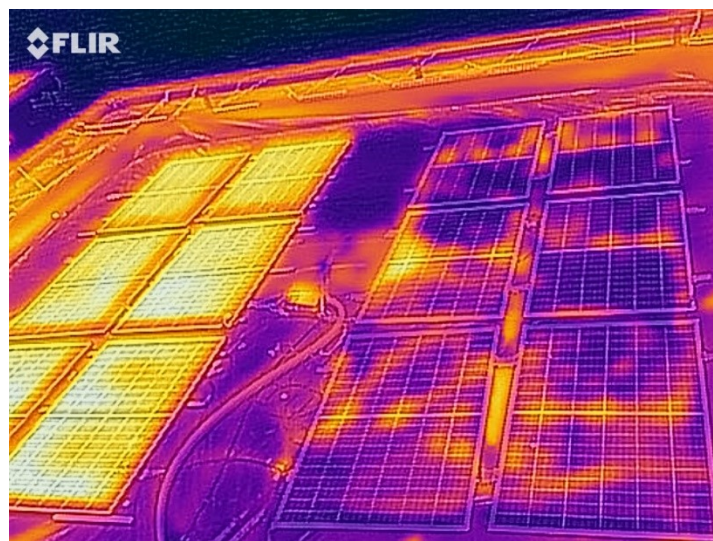


Figure 3.12 (Ocean Sun, by permission): IR picture of the experimental setup in Singapore. Reference modules with frame, lifted by wooden lists to the left and laminates in thermal contact with water to the right.

3.2.2 Insolation and temperature at the test site

The average annual global horizontal irradiation at the meteorological station at Singapore Airport is approximately 1600 kWh/m² (JRC EC, 2017). As illustrated by Figure 3.13, the monthly average irradiation is approximately equal throughout the year, making Singapore a suitable site for horizontal PV modules.

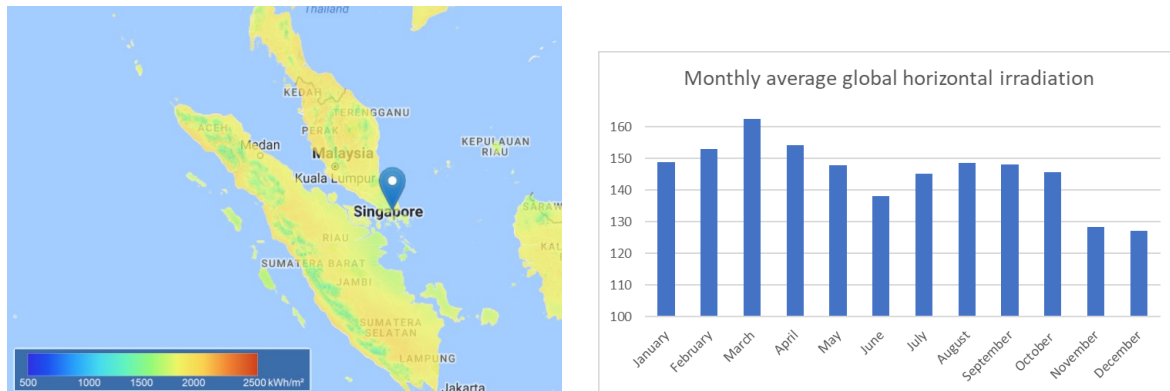


Figure 3.13 Top: Map over irradiation for Singapore, giving an average at approximately 1600 kWh/m² per year. Bottom: Monthly global horizontal average for Singapore Airport (JRC EC, 2017)

Long term measurements of ambient temperature are illustrated by Figure 3.14. The average water temperature is also included in the figure.

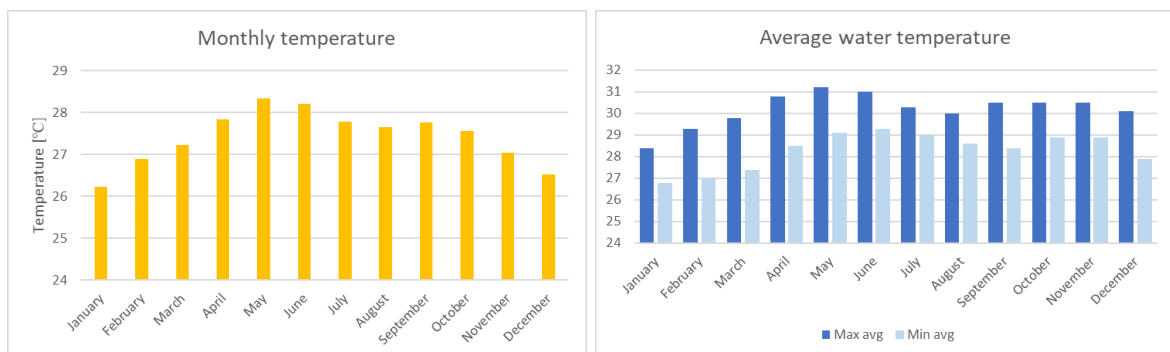


Figure 3.14: Left: Monthly average ambient temperature for Singapore Airport (JRC EC, 2017). Right: Average maximum and minimum water temperature for Singapore (World sea temperature, 2018).

3.3 Data analysis

This subchapter describes how the data from the test site at Kjeller is selected, adjusted and presented.

3.3.1 Data selection

Data from 10.04.18 to 15.04.18 is chosen for the analysis. The data from these dates are assumed to be sufficient for the analysis, as the days were somewhat similar in irradiation and temperature. It would arguably have been beneficial for the measurements to be conducted in the summer months, with even higher irradiance and ambient temperature. Due to the timeframe of the thesis, this was not possible. Additionally, the weather condition was assumed to be inadequate before this period. Hence the best possible dates were chosen to represent the test period.

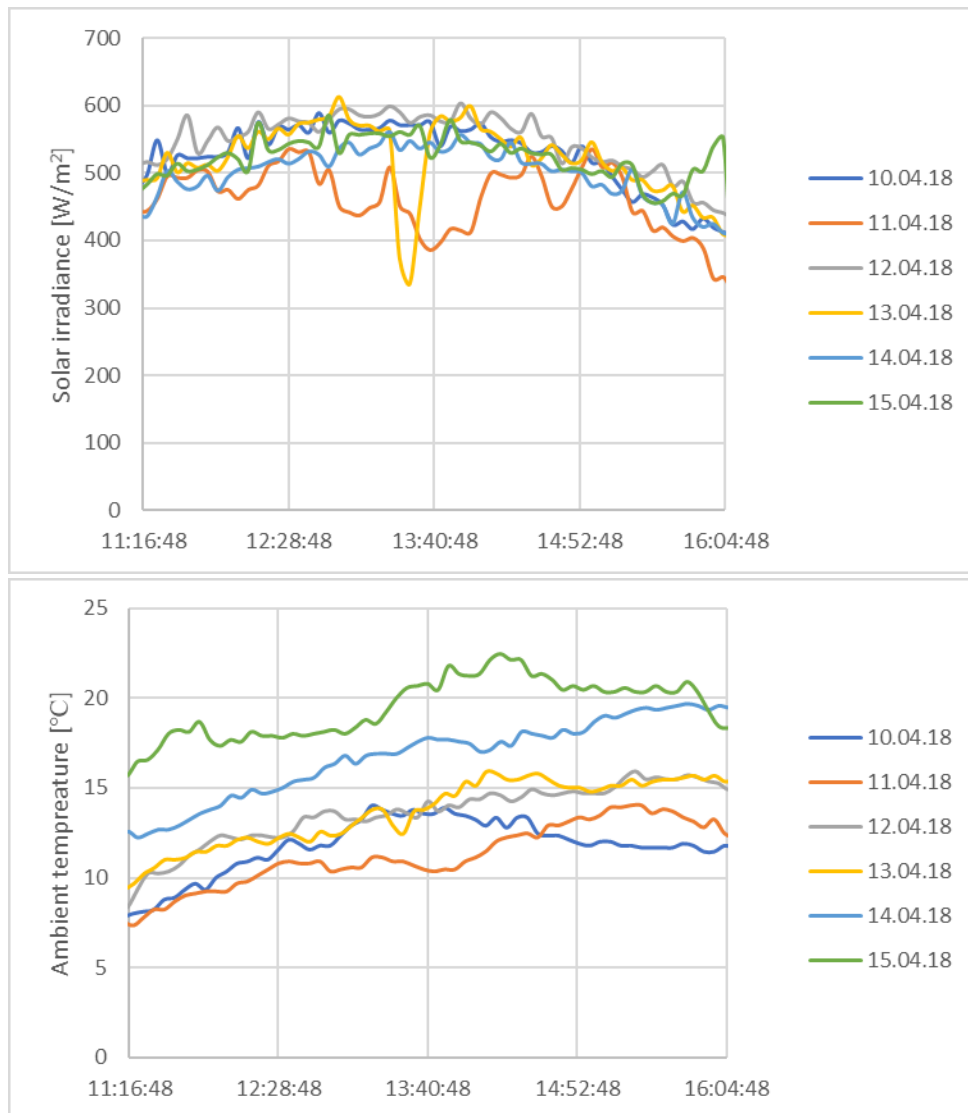


Figure 3.15: Top: Solar irradiance for the test period. Bottom: Ambient temperature measured at the test site at IFE, for the test period.

Furthermore, it was chosen to limit the analysis to a specific time interval, to exclude measuring errors and ensure as equal conditions as possible for both modules. Due to the surrounding buildings, both modules and the reference cell experienced shading until between 11.00 and 11.15, in which they were finally hit by direct irradiance.

The temperature sensors measuring back-surface module temperature were disconnected between 16.00 and 17.00 for the two test days; Tuesday 10.04.18 and Thursday 12.04.18. Some shade was casted over the modules when the sensors were disconnected, causing the modules to experience different conditions. In addition, the solar altitude decreases in the evening, presumably leading to different conditions for the modules. Thus, the time interval ranges from 11.15 to 16.00.

For a detailed analysis, Tuesday 10.04.18 and Thursday 12.04.18 were chosen, based on the weather forecast for those days and the availability of the temperature sensors. In addition to being the days when back-surface temperature was measured, the irradiance was the highest during the test period for those days. It would have been beneficial to conduct measurements of the back-surface temperature throughout the test period.

The collected data is

- Global horizontal irradiance
- Ambient temperature
- Reference module power output
- Floating module power output
- Back-surface module temperature (10.04.18 and 12.04.18)

3.3.2 Data adjustment

3.3.2.1 Power output

To correctly compare the power output from the modules, their difference in initial performance must be considered. The modules will not perform identically due to small differences in efficiency amongst modules with the same nominal power. The power of the two modules, P_{max} , were measured under STC conditions in the solar simulator.

Because the time stamps of the logging of the global horizontal irradiance and module power output were not synchronized, the actual performance ratio for each five-minute interval cannot be accurately calculated. However, the two modules may be compared directly as the irradiation conditions are identical with no shadows over the chosen time frame.

By dividing the power output by the expected maximum power output, P_{max} , the modules can be compared fairly. This is called *normalized power output*:

$$P_n = \frac{P_{out}}{P_{max}} \quad (24)$$

3.3.2.2 Cell temperature

Figure 3.16 illustrates the cell temperatures, estimated from equation 6 and 7. It describes the errors in using the ambient temperature, as the estimated cell temperature is equal for both modules. Thus, the measured back-surface temperature is used to derive the cell temperature of both modules, from equation 6. The uncertainty in the cell temperature is assumed to be that of the back-surface temperature.

$$T_c = T_m + \frac{I_L}{I_{L0}} \Delta T \quad (6)$$

$$T_c = T_{amb} + \frac{NOCT - 20}{800} I_L \quad (7)$$

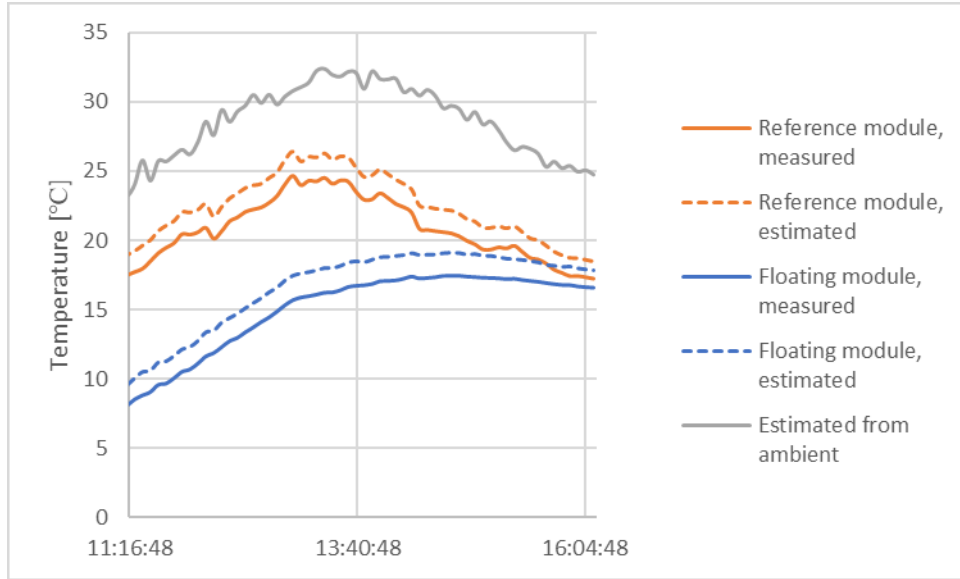


Figure 3.16: Illustration of cell temperatures estimated from measured back-surface temperature and measured ambient temperature, from Tuesday 10.04.18.

3.3.2.3 The U-value

The U-value is calculated from measured irradiance, ambient temperature, module efficiency and cell temperature, as illustrated by equation 14. These values are not logged synchronically.

$$U = \frac{G_{hor}(1 - \eta)}{T_c - T_{amb}} \quad (14)$$

However, the loggings are only a few minutes off, and for the two test days in which the U-value is calculated, the irradiance and ambient temperature were quite stable, as illustrated in the figure below. Furthermore, the errors are assumed to be equal for both modules. Thus, it is assumed that the errors are negligible.

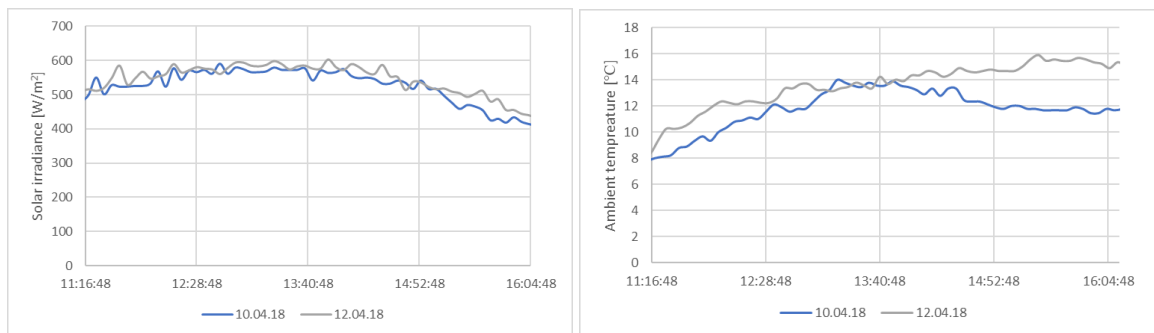


Figure 3.17: Left: Solar irradiance for Tuesday 10.04.18 and Thursday 12.04.18. Right: Ambient temperature for Tuesday 10.04.18 and Thursday 12.04.18. The irradiance and ambient temperature are rather stable throughout the time interval for both test days.

Additionally, as illustrated by Figure 3.16, the temperature of the floating module is rather stable. Thus, there are even less fluctuations for the floating module, which is the most important module for calculating the cooling effect.

In a more optimal setup, the logging of the measurements should be synchronized.

3.3.3 Presentation of results

3.3.3.1 Performance

The performance of both modules is given, and the relative change in normalized power output is calculated and presented for the given time interval.

3.3.3.2 Back-surface module temperatures

The back-surface temperature of each module is compared against one another for the two test days in which the sensors were connected. It is also compared to the ambient temperature. In addition, the back-surface module temperatures are plotted against irradiance and ambient temperature, to illustrate what affects each module.

Lastly, IR pictures are presented to illustrate the module temperatures.

3.3.3.3 The U-value

When the cell temperature is estimated, the U-value can be estimated for the two days with back-surface temperature measurements by equation 14. The uncertainty of the U-value is related to the uncertainty in the measurements at the test site and the arguments presented in the previous subchapter.

3.3.4 Summary of data analysis

A summary of the data analysis, from the experiment at IFE, is presented in Figure 3.18.

Data selection	Data adjustment	Data presentation
<ul style="list-style-type: none">• Test period: 10.04.18 – 15.04.18• Time interval: 11.15 – 16.00• Detailed analysis: 10.04.18 & 12.04.18	<ul style="list-style-type: none">• Normalized power output• Cell temperature estimated from back-surface	<ul style="list-style-type: none">• Difference in normalized power output• Module temperatures• U-value

Figure 3.18: Summary of the data analysis; data selection, adjustment and presentation.

3.4 Mathematical methodology

This chapter describes the background, structural setup and parameters for the thermal model. The purpose of the developed model is to predict results from a floating PV. MATLAB is the software used for this purpose.

3.4.1 Background

For the thermal modeling, the theory from chapter 2.4 have been applied. The intention of the model is that it can be used for any configuration of technologies, in which materials and material properties can be modified.

As illustrated in Figure 2.6, heat transfer occurs as heat convection, heat conduction and radiation. Radiation is neglected because it has very little impact on the overall heat loss. On a sunny day, with irradiance at 500 W/m², measured back-surface module temperature at 24°C and ambient temperature at 14°C, the radiation loss accounts for less than 0.1 % of the total heat loss. This is based on measurements from the test site at Kjeller.

Considering that the silicon cell is in the center of the module, there are resistance on each side that work in series. The thermal resistances depend on the materials in which the heat must traverse, in addition to the surrounding fluid(s). Heat transfer to air from the front side and to water (or air) from the back side are parallel processes. Thus, the equation for heat transfer ends up being:

$$Q = \frac{T_c - T_{amb}}{R_f} + \frac{T_c - T_{water}}{R_b} \quad (27)$$

where R_f is the front resistance, R_b is the back resistance, T_c is the cell temperature, T_{amb} is the ambient temperature and T_{water} is the water temperature.

For a PV module, the front resistance will be calculated from the following equation:

$$R_f = R_{f1} + R_{f2} + \dots R_{f-n} + R_{convecton_to_air} \quad (28a)$$

$$R_{front} = \frac{L}{kA_{f1}} + \frac{L}{kA_{f2}} + \dots \frac{L}{kA_{f-n}} + \frac{1}{h_{air}A} \quad (26b)$$

where h_{air} is the forced convection heat transfer coefficient, k is the thermal conductivity, L is the thickness of the material and A is the surface area.

The back resistance for the floating module will be calculated from the equation:

$$R_b = R_{b1} + R_{b2} + \dots R_{b-n} + R_{convecton_to_water} \quad (29a)$$

$$R_{back} = \frac{L}{kA_{b1}} + \frac{L}{kA_{b2}} + \dots \frac{L}{kA_{b-n}} + \frac{1}{h_{water}A} \quad (27b)$$

where h_{water} is the convection heat transfer coefficient, which is highly dependent on the water's behavior and contact areas between the two surfaces. For the reference module, with air circulation on the back side, convection for air would be included instead of convection by water for the back resistance.

Combining equation 12 and 27 gives an expression for the cell temperature:

$$T_c = \frac{G_{hor}(1 - \eta) \times A \times R_f R_b + T_{amb} R_b + T_{water} R_f}{R_f + R_b} \quad (30)$$

where G_{hor} is the global horizontal irradiance incident on the module's surface, A .

Thus, when the air temperature, water temperature, wind speed and the irradiance at the is measured, the cell temperature can be calculated and compared to the measured cell temperature.

As discussed in subchapter 2.3.4.2, the efficiency is dependent on module temperature. By inserting equation 30 into equation 9, an expression for the efficiency arise:

$$\eta = \frac{\eta_{STC} [R_f + R_b - \beta G_{hor} A R_f R_b - \beta T_{amb} R_b - \beta T_{water} R_f + \beta T_{STC} (R_f + R_b)]}{R_f + R_b - \eta_{STC} \beta G_{hor} A R_f R_b} \quad (31)$$

The expected power output can now be calculated by equation 10 or by simply using the relationship:

$$P_{out} = \eta G_{hor} A \quad (32)$$

3.4.2 Structural setup

The structures, materials and configuration of the PV modules are of importance for the thermal model. Table 3.2 presents some general information about the PV module used at the test site at Kjeller, while the material properties are presented in Table 3.3.

Table 3.2: General information and materials for the PV module used at the test site at Kjeller; REC Peak Energy.

	270W REC Peak Energy
Test site	IFE at Kjeller
Module area [m²]	1.65
Front glass	Tempered glass with high transmittance
PV cells	Multi-crystalline silicon
Backsheet	Highly resistant polyester
Canvas	Commercial tarp

Table 3.3 Material properties for composition of REC (Liu et al., 2017; The Engineering ToolBox)

Material	Layer	Thickness L [m]	Thermal conductivity k [W/mK]
Glass	Front glass	0.0032	0.7
EVA	Encapsulant	500×10^{-6}	0.311
Silicon	Silicon cell	200×10^{-6}	130
Laminate	Backsheet	300×10^{-6}	0.15
Tarp	Canvas	200×10^{-6}	0.5

3.4.3 Parameters

This subchapter describes the challenges related to defining the parameters of the thermal model.

3.4.3.1 Convective coefficients

Convection by wind occurs on the top surface of both PV modules, and on the bottom surface of the reference module. Zhou et al. (2015) suggests that the cell temperature decrease rapidly at lower wind speeds (typically under 10 m/s), but that high wind speed is helpful for the improving of solar cell electrical efficiency. The biggest impact in module temperature happens when the wind increases from 0 to 1 m/s. Thus, low ambient temperatures and high wind speed is recommended for better performance of PV modules.

For an offshore installation, it is likely that only forced convection will occur, as the wind speeds typically are higher at sea than onshore. For the test site at IFE, the modules are protected from wind by surrounding buildings, reducing the impact of the wind.

Armstrong and Hurley (2010) gives a summary of various values for the coefficient h_{forced} at different wind speeds. A common equation is given by:

$$h = 2.56v + 8.55 \quad (33)$$

where v is wind speed. A typical value for the free convective heat transfer coefficient for air is approximately 2-25 W/m²K (Bergman et al., 2011).

Convection by water occurs on the bottom surface of the floating PV module. For simplicity, it is assumed that the water has a constant convective heat coefficient and that the material is uniform and moves only in one direction, in a laminar manner (no turbulence).

The temperature of the water is also assumed to be constant, and as the ocean is big, the temperature does not rise due to the heat removed from the solar module.

Table 3.4 Properties of freshwater (10 °C) and seawater (20 °C, 3.5 % salinity) at atmospheric pressure (Denny, 1993)

	Specific heat capacity c [J/kg·K]	Thermal expansivity β [K ⁻¹]	Thermal conductivity k [W/m K]	Density ρ [kg/m ³]	Dynamic viscosity μ [kg/m·s]	Kinematic viscosity ν_k [m ² /s]	Prandtl number Pr
Seawater	4182	0.2572×10^{-3}	0.6011	1024.76	1.09×10^{-3}	1.06×10^{-6}	7.62
Fresh water	4192	0.0881×10^{-3}	0.5867	999.73	1.310×10^{-3}	1.31×10^{-6}	9.36

Following the equations in subchapter 2.4.2 and values given in the table above, the forced convective coefficient for the ocean ranges around 1000 W/m²K.

For the experimental setup at IFE, there is assumed to be free convection at the bottom surface of the floating module, as the water essentially is stationary. The water depth is approximately 40 cm and the water temperature is approximately 4°C. The temperature is assumed to be somewhat lower at the bottom. Following the equations in subchapter 2.4.2 for natural convection and the properties in Table 3.4, the free convective heat transfer coefficient is approximately 500 W/m²K.

Calculating the correct heat transfer coefficient for a real test site is very complex, and there are several factors that affect the real value. For an experimental setup as described above, junction boxes and cables on the back side of the modules will hinder the thermal contact with the canvas and hence the water. In addition, it is very likely that air gaps will occur between the canvas and the water, leading to even lower thermal contact. The roughness of the canvas will also have an impact on the thermal contact, in addition to possible folding.

3.4.3.2 Wind speed

As previously discussed, there are no measurements for wind speed or wind direction at the test site, and the test site at IFE is well protected from wind. Furthermore, when there is effective water cooling,

the cooling effect from wind is negligible, as water has several times higher conductive heat transfer coefficient than air.

3.4.3.3 *Water temperature*

Even though the sea temperature is assumed to be constant, this is likely not applicable for the water in the inflatable pool at IFE. The water temperature on Tuesday 10.04.18 was almost constant at 4°C. However, at Thursday 12.04.18, the temperature increased during the day. As the temperature was measured to approximately 4°C several times during several consecutive days, it was decided to use this as the input for the thermal model.

3.4.3.4 *Overall thermal resistances*

The overall thermal resistance for the back side is increased in the thermal model for several reasons:

- The contact between each material within the solar module is likely to not be entirely ideal, increasing the thermal resistance between each material.
- The contact between the PV module and the canvas is affected by the junction box, cables and folds in the canvas, consequently reducing the thermal contact and increasing the thermal resistance.
- The temperature sensors at the back side of the module reduce the thermal contact with the canvas even further. In addition, the connection between the sensors and the module is likely to not be ideal.
- The contact between the canvas and the water is affected by folds in the canvas, reducing thermal contact and increasing the thermal resistance.

Some of these arguments apply for the front resistance as well, but as this resistance is equal for both the reference and the floating module, it is assumed to be negligible.

There is much uncertainty related to all the points above, but there is no way to quantify these uncertainties, other than by experimental testing.

For the reference module, the back resistance is affected by air cooling. As the module is very close to the ground, it is argued that the convection is smaller than on the front side.

3.4.4 Presentation of results and summary

The estimated power output, efficiencies, cell temperatures and U-value are calculated by the thermal model. The results are presented and compared to the experimental data from the test site at IFE. To evaluate the thermal model, estimations for both the reference module and the floating module is seen as significant.

The thermal loss coefficient, U , calculated from the thermal model is based on equation 14.

3.5 Computational methodology

An important part of this thesis is to use computer modeling tools to simulate the behavior and performance of floating PV modules. This is done by modifying terrestrial installations, as no software can simulate floating installations (to the authors knowledge).

For the software tools, TRNSSYS and PVsyst have been chosen. The results from the simulations are compared to the experimental results from the test site at Kjeller.

3.5.1 PVsyst

PVsyst is a photovoltaic software tool used to create, analyze and evaluate different configurations of PV technology (PVsyst SA, 2012). It is well known in the PV industry. PVsyst version 6.5.4 has been used in this thesis. Each step of the simulation is carefully explained in the sub chapters.

The simulated test site is created to replicate the real test site as good as possible. One project was created for each day of simulation, and two variants for each project; reference module variant and floating module variant.

Site and meteorological file. As there is no site for Kjeller in PVsyst, a site was created manually at latitude 59.97 and longitude 11.05. This creates an interpolated meteorological data file from Meteonorm 7.1 (1991-2010). However, the measurements from IFE were used as input, by importing an ASCII file with real weather data to PVsyst. It was checked that PVsyst reads the values correctly.

Orientation. As with the experimental setup, the modules were positioned with 0° tilt, and azimuth 0°. The orientation angle is, as previously discussed, not important as the modules are not tilted.

System. The module used at the test site is the 270W REC Peak Energy module. This had to be manually created in PVsyst, and was done by modifying the 260W REC Peak Energy module. Parametric values (“manufacturer specifications or other measurements”) were taken from the data sheet for the “*Basic data*” header. In the “*Model parameter*” header, the shunt resistance and series resistance was changed according to the equivalent circuit that require five parameters. These were calculated by the Engineering Equation Solver given as a tool by the TRNSSYS license (F-Chart Software, 2018). The temperature coefficient for P_{MPP} was also changed according to the datasheet.

The inverter chosen for the simulation is the same one as used in the experiment, the AP Systems YC500I-EU microinverter.

Global System configuration

1 Number of kinds of sub-arrays

Global system summary

Nb. of modules	1	Nominal PV Power	0.3 kWp
Module area	2 m ²	Maximum PV Power	0.2 kWdc
Nb. of inverters	0.5	Nominal AC Power	0.3 kWac

PV Array

Sub-array name and Orientation

Name: PV Array

Orient: Fixed Tilted Plane

Tilt: 0°

Azimuth: 0°

Presizing Help

No Sizing

Enter planned power: 0.3 kWp

... or available area: 2 m²

Select the PV module

Available Now

REC 270 Wp 26V Si-poly REC 270PE / PE-BLK Since 2014 Manufacturer 2C

Sizing voltages: V_{mpp} (60°C) 27.4 V

V_{oc} (-10°C) 42.0 V

Select the inverter

Available Now

APsystems 0.50 kW 22 - 45 V HF Tr 50 YC500I-EU Since 2015

Nb of MPPT inputs: 1

Operating Voltage: 22-45 V

Global Inverter's power: 0.3 kWac

Input maximum voltage: 55 V

Design the array

Number of modules and strings

Mod. in series: 1

Nbre strings: 1

Overload loss: 0.0 %

P_{nom} ratio: 1.08

Nb. modules: 1

Area: 2 m²

Operating conditions

V_{mpp} (60°C): 27 V

V_{mpp} (20°C): 32 V

V_{oc} (-10°C): 42 V

Plane irradiance: 1000 W/m²

I_{mpp} (STC): 8.6 A

I_{sc} (STC): 9.2 A

I_{sc} (at STC): 9.2 A

Max. operating power at 1000 W/m² and 50°C: 0.2 kW

Array nom. Power (STC): 0.3 kWp

Figure 3.19: System configuration used for PVsyst simulations.

Detailed losses. The “global wiring resistance” under the header “Ohmic losses” was set to zero, as the wires of the real system are negligible (short). Under “Module quality – LID – Mismatch”, all parameters were set to zero as well. This is mainly because only one module is simulated at a time. As the modules used in the experiment were flash tested, it is also assumed that taking the ideal module for the simulation, causes negligible errors or differences.

The “*Thermal parameter*” was changed for the simulations, to represent actual thermal losses. The actual thermal losses were calculated from the measured irradiance, effect, ambient temperature and cell temperatures for each day.

The *constant thermal loss factor*, U , initially had its default maximum value set to 50 W/m²K. This was changed by “Preferences”, “Edit hidden parameters”, “System design parameters”, setting the “heat loss factor maximum value” to a higher value.

Shading. No shading was included in the simulation. The surrounding buildings could have been included, but as the analysis only considers the time interval specified in subchapter 3.3.1, that was argued to be insignificant.

Simulation and analysis. For each variant in each project, hourly values are generated and exported to an Excel-file, in which it is processed. The simulation creates an output file with *horizontal global irradiation*, *ambient temperature*, *wind velocity*, *average module temperature during running* (cell temperature), *available energy at inverter output* and *performance ratio*. This is then compared to the actual, measured values from the specific day of simulation.

3.5.2 TRNSYS

TRNSYS is a flexible software used to simulate the behavior of transient systems, mainly focusing on assessing the performance of thermal and electrical energy systems (TRNSYS, 2018). It works by connecting individual component models, called Types, together in a model.

Similar to PVsyst, the simulation with TRNSYS is created to simulate the real test site. Two projects were created for each day; one reference model and one model for the floating module. The parameters are equal for all projects, and the wind speed is the only variable that varies from each project.

TRNSYS cannot model thermal losses for PV modules the same way as PVsyst. However, as explained by subchapter 2.4.1, equation 15 can be written as equation 13, for a given PV module. As the average U-value is calculated from the measurements at the test site at Kjeller, the average wind speed can be derived from equation 13. Two simulations are run for the reference module, in which one ignores wind altogether and one takes the wind speed given by equation 13 and the U-value from the test site. Furthermore, one simulation is run for the floating module, where the wind speed is derived as above.

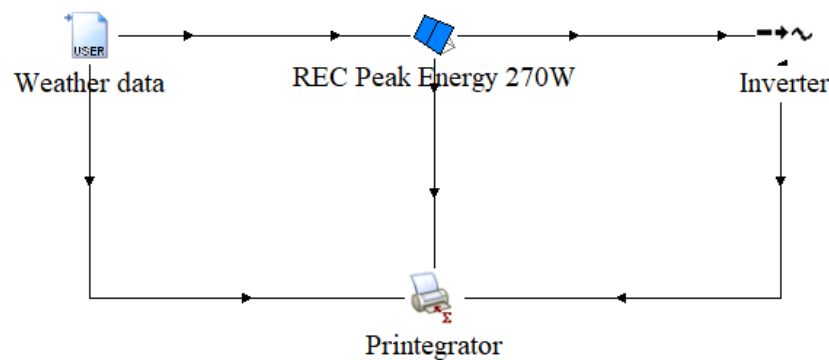


Figure 3.20: TRNSYS system configuration for simulation of IFE experiment

Weather data. Weather data is imported from Excel, consisting of measured global horizontal irradiance and ambient temperature from the test site at Kjeller. The data gives values at an interval of five minutes. TRNSYS component Type 9a was used to read the files. It was checked that the component reads the input values correctly.

The weather data also gives wind speed as an input, in which the value is based on the discussion above.

PV module and inverter. The PV chosen is component Type 190c; the advanced model, with MPP tracking and no inverter. The parameters are defined according to the datasheet and the Engineering Equation Solver is used to calculate the five parameters from the equivalent circuit (F-Chart Software, 2018).

TRNSYS component Type 48a is the inverter. The inverter efficiency is assumed to be 95 %, as the microinverter from the test site operate at a maximum of 95.5 %. If the inverter is overestimated, the outputs from both modules will have the same error, but the difference will be independent of the inverter.

Printegrator. TRNSYS component Type 46a was chosen for printing the results and subsequent data analysis in Excel.

Simulation and analysis. The simulation creates hourly output data which is exported and analyzed in Excel. The outputs from the printegrator is *solar irradiance, power output from inverter, ambient temperature, module temperature* (cell temperature) and *wind speed*. These values are compared to the experimental results from the test site at Kjeller.

3.6 Summary of methodologies

Figure 3.21 summarizes the methodologies and the presentation of results. Firstly, the experimental methodology gives the difference in normalized power output, back-surface module temperatures and U-values from the experiment conducted at Kjeller. Secondly, the mathematical methodology presents estimated results based on measured data from the test site at Kjeller. Lastly, the computational methodology presents simulated results based on measured data from the test site at Kjeller, simulated by PVsyst and TRNSYS. The results from each estimation and simulated is consequently compared to the experimental results.

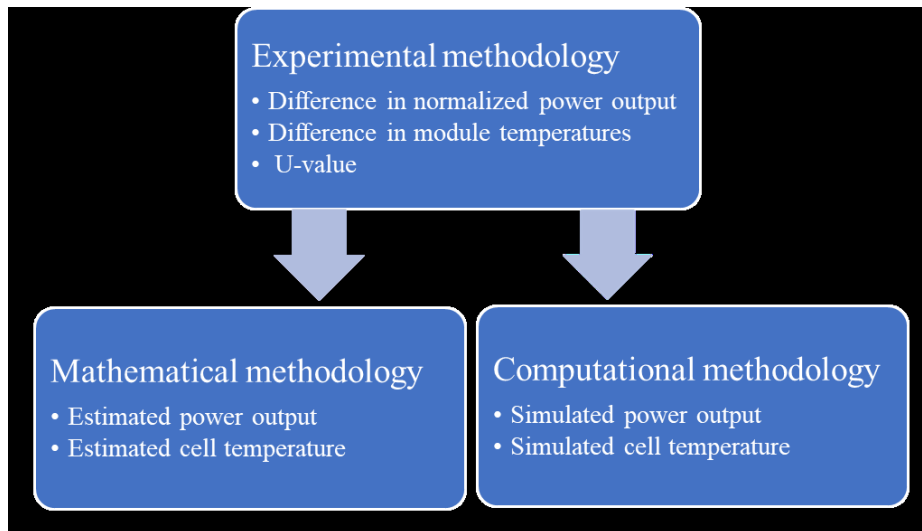


Figure 3.21: Summary of methodologies and presentation of results.

4 Results and discussion

The first part of this chapter presents the experimental results from the test site at Kjeller. The second part presents the results from the thermal modeling based on the test site at Kjeller, and discusses the viability of the model. The third part presents the results from simulations by PVsyst and TRNSYS, respectively, and discusses the software programs' ability to correctly simulate floating PV modules.

4.1 Experimental results from IFE, Kjeller

4.1.1 Performance

The floating module has higher normalized production than the reference module, for the test interval on each test day, ranging between 2-6 %. Table 4.1 illustrates the average, maximum and minimum difference in performance, and Figure 4.1 illustrates the variations for each test day. The sudden change in relative performance of the modules Saturday 14.04, is likely caused by shade due to human activity close by the test site (represented by the high maximum difference).

Figure 4.2 illustrates measured power output and solar irradiance each day of the test period. It provides a general and detailed overview of each day, illustrating why the test interval was chosen.

Table 4.1: Summary of difference in normalized power output for the test period (and test interval: 11:15 – 16:00)

Test day	Tuesday 10.04	Wednesday 11.04	Thursday 12.04	Friday 13.04	Saturday 14.04	Sunday 15.04
Average difference [%]	3.3	2.9	4.1	3.3	3.5	4.4
Maximum difference [%]	4.4	4.5	5.9	4.2	9.8	5.4
Minimum difference [%]	2.2	1.8	2.8	2.2	1.9	3.1

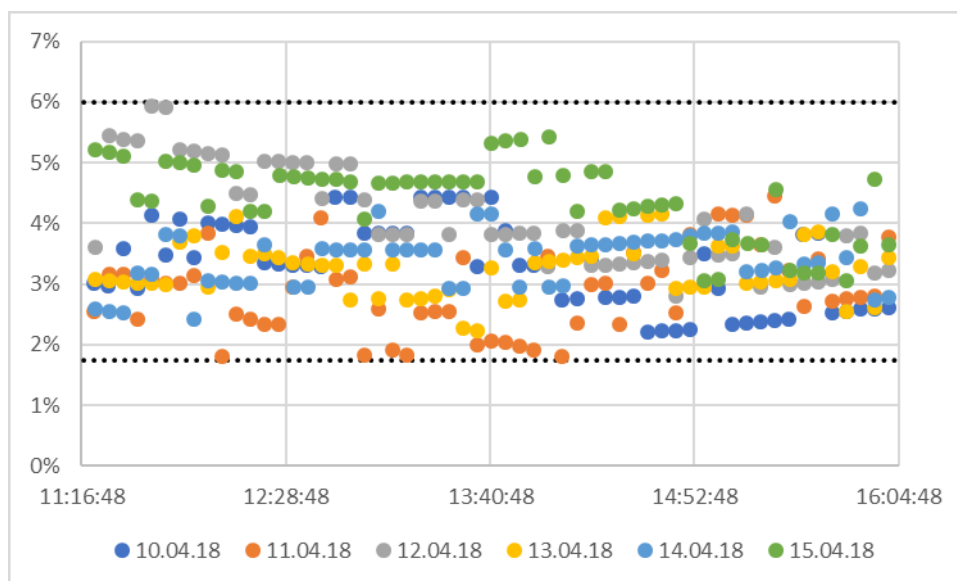


Figure 4.1: Difference in normalized production for the test period and test interval. The floating module has generally 2-6 % higher normalized power output than the reference module.

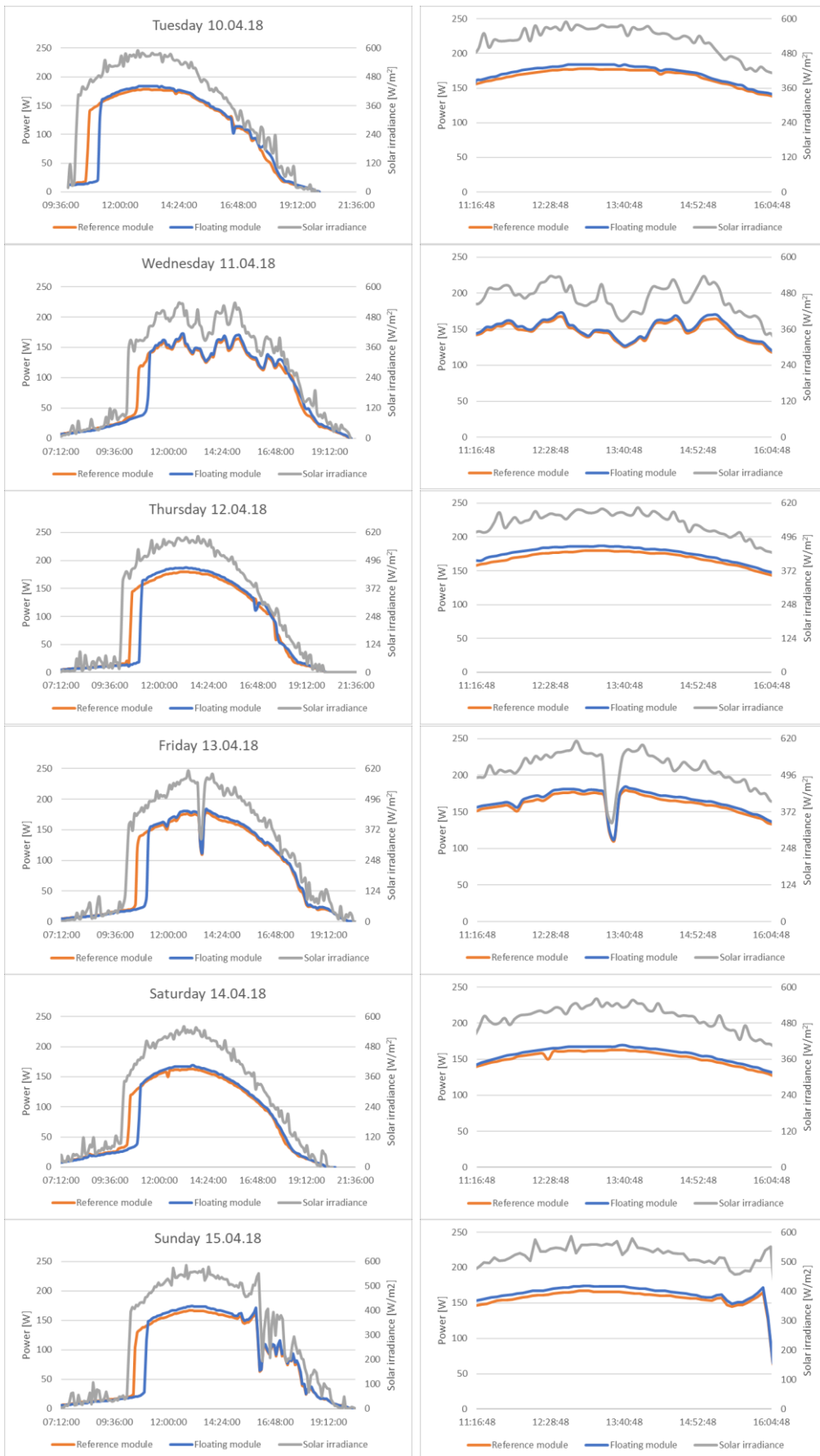


Figure 4.2: Left: General overview of measurements from test site at IFE. Right: Detailed overview of measurements.

4.1.2 Back-surface module temperature

4.1.2.1 Comparison of test days

Figure 4.3 illustrates the back-surface temperatures and the ambient temperature for the time interval of the two test days in which temperature sensors were connected. It is evident that the reference module has higher back-surface temperature than the floating module for the test period. The average temperature for the reference module is 19.8°C, while the average temperature for the floating module is 12.3°C for Tuesday 10.04.18. On Thursday 12.04, the average temperature for the reference module is 22.7°C and the average temperature for the floating module is 15.2°C.

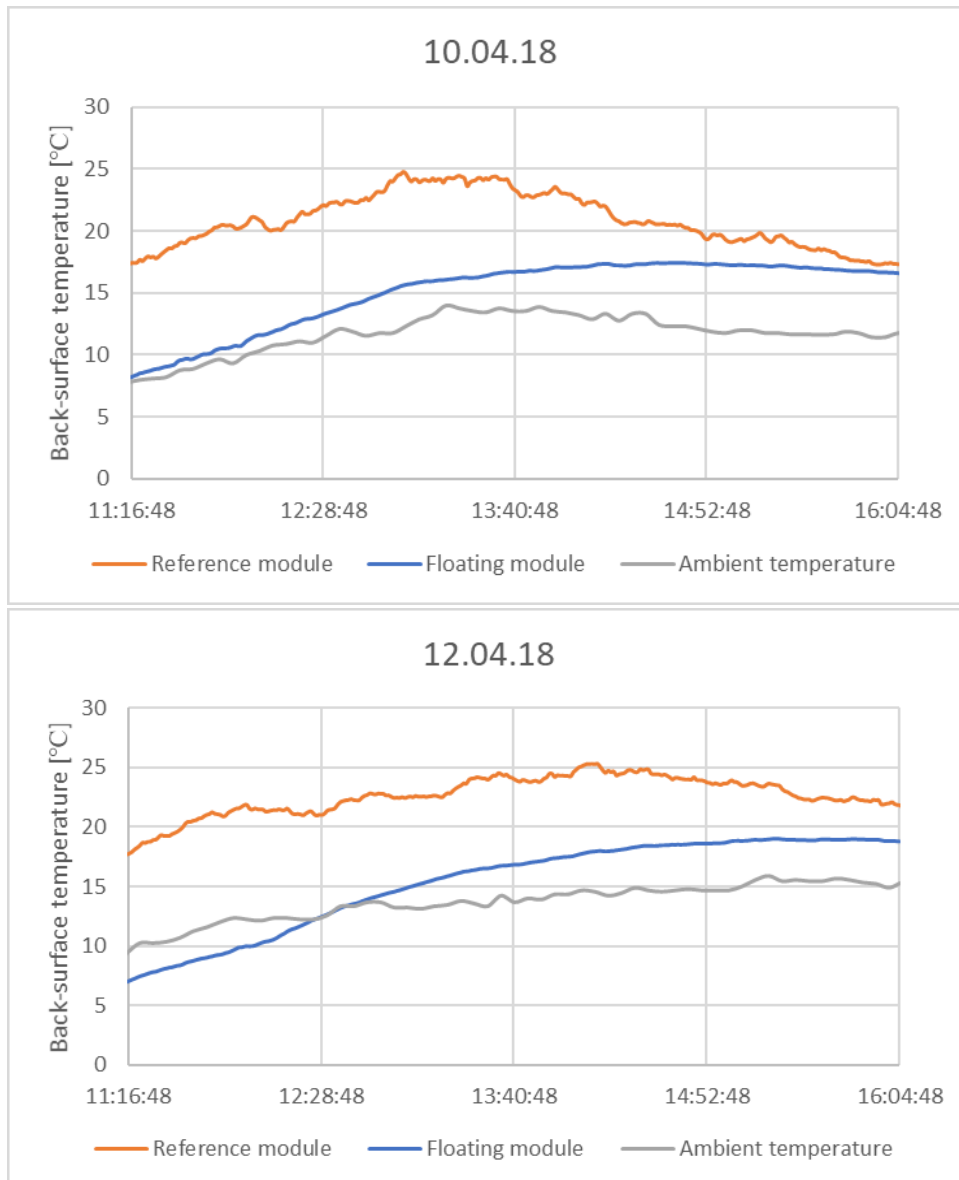


Figure 4.3: Back-surface module temperature for reference module and floating module, and measured ambient temperature. Top: Tuesday 10.04.18. Bottom: Thursday 12.04.18. The night to Thursday was quite cold, with -7°C, causing the floating module to be colder than the ambient until mid-day.

Figure 4.4 illustrates the difference in back-surface temperatures between the reference and the floating module. The difference decreases during the test interval for both test days. The temperature difference is larger on Thursday 12.04, in which the ambient temperature also is higher. For further analysis, longer measurements would be beneficial.

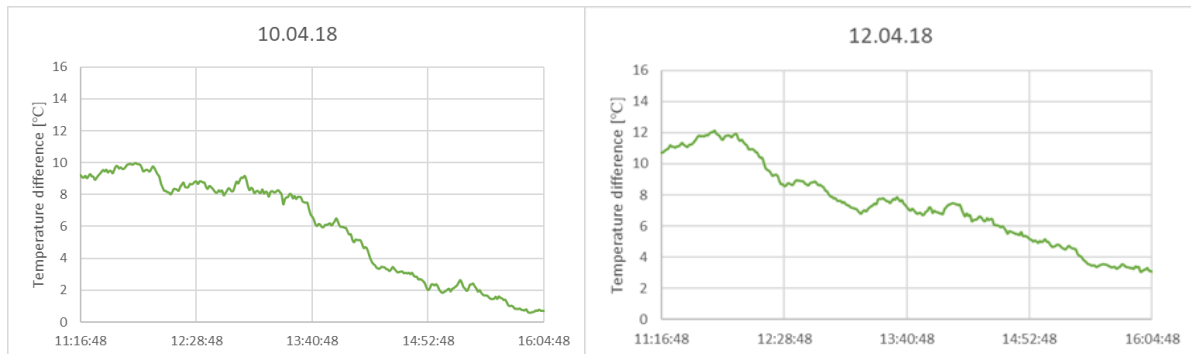


Figure 4.4: The difference in back-module surface temperature between the reference module and the floating module. It is evident that the reference module's temperature is higher than the floating module's temperature for the test interval. Left: Tuesday 10.04. Right: Thursday 12.04.

Table 4.2 presents the average, maximum and minimum differences in measured back-surface temperatures. The differences are based on the time interval and figures above.

Table 4.2: Average, maximum and minimum temperature difference between the reference module and the floating module for both test days.

	Tuesday 10.04	Sunday 15.04
Average difference [°C]	5.92	7.45
Maximum difference [°C]	9.97	12.2
Minimum difference [°C]	0.58	3.07

Figure 4.5 illustrates the relationship between back-surface temperature and ambient temperature. It is indicated that the floating module's temperature is linear with ambient temperature, while the reference module's temperature is less linear. As illustrated in Figure 4.3, the reference module temperature follows the behavior of the ambient temperature more closely than the floating module temperature, for both test days.

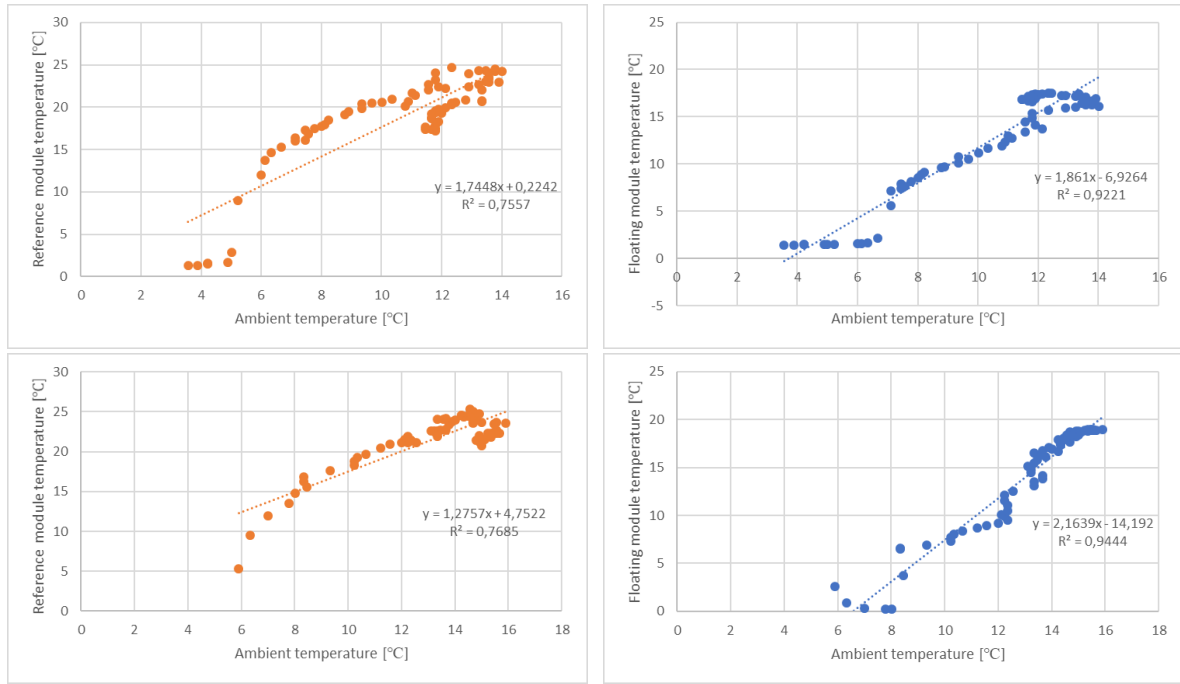


Figure 4.5: Back-surface module temperature plotted against ambient temperature. Top left: Reference module, 10.04. Top right: Floating module, 10.04. Bottom left: Reference module, 12.04. Bottom right: Floating module, 12.04.

Figure 4.6 illustrates the back-surface temperatures at measured irradiances. It is clear that the temperature of the reference module is more affected by the irradiance than the temperature of the floating module. When the irradiance decreases, the temperature of the reference module decreases at a higher rate than that of the floating module. This is expected due to the greater heat capacity of water, which is about four times higher than air. The floating module does not respond as quickly to changes in irradiance, because the water keeps the temperature more constant.

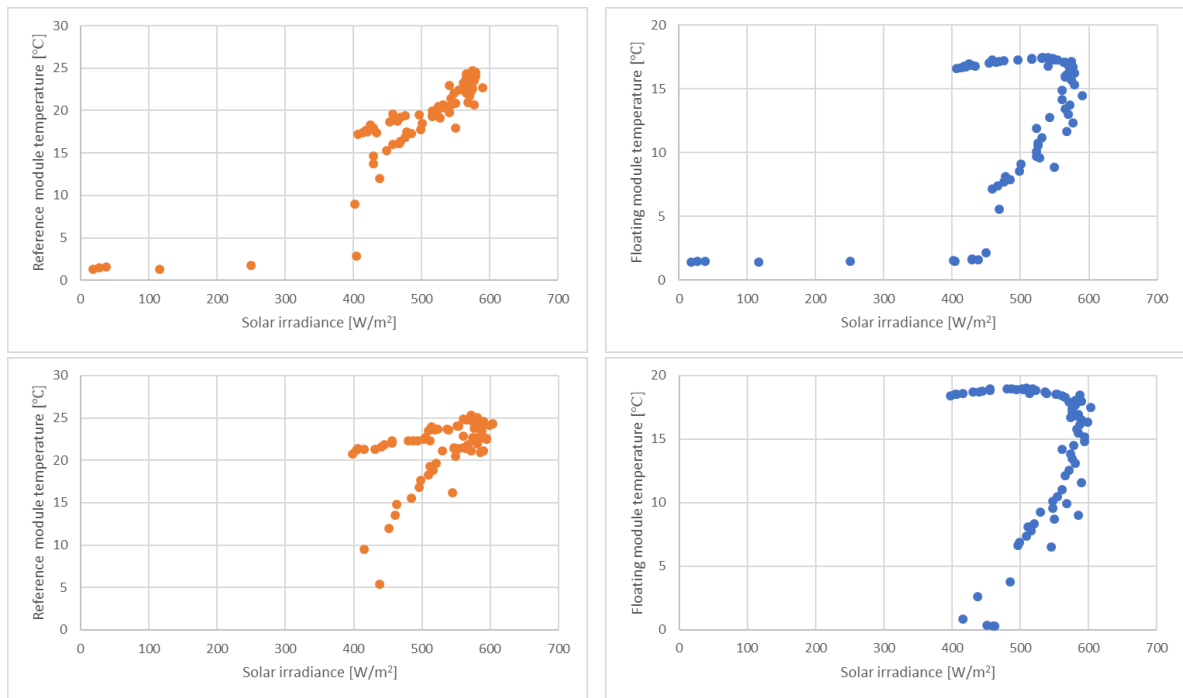


Figure 4.6: Back-surface module temperature plotted against irradiance. Top left: Reference module, 10.04. Top right: Floating module, 10.04. Bottom left: Reference module, 12.04. Bottom right: Floating module, 12.04.

4.1.2.2 IR pictures

IR pictures were taken to study the variation in temperature over the modules, and to get an independent measurement of temperature, as this is a crucial parameter for these experiments. The pictures were taken Tuesday 10.04, at approximately 13.00. As indicated by Figure 4.4, the measured temperature difference was approximately 8°C at that time.

The absolute temperature of the IR camera is not correctly calibrated, but it is very useful to look at the relative difference in temperature. The pictures imply a temperature difference of about ten degrees. However, there are local temperature gradients within each module, as shown by Figure 4.7.

For the floating module, warmer spots appear, mainly caused by the junction box and cables at the far side of the module. Also, the temperature sensors connected to the back side of the module cause a local increase in temperature. In addition, it might look like there are some uneven structures, leading to higher temperatures. These are evident as the “horizontal lines” crossing the module. If this is the case, then it supports the statement saying that the thermal contact is not perfect between materials and that the thermal resistances are higher than estimated for an ideal setup. However, these lines might also be related to the strings of cells in the module. More pictures would arguably be beneficial for further evaluation.

For the reference module, the temperature seems to be more evenly distributed across the surface area. The bottom left shows a higher temperature, which could be due to the closer proximity to the ground, leading to less air cooling. However, the differences might also be caused by some reflection issues.

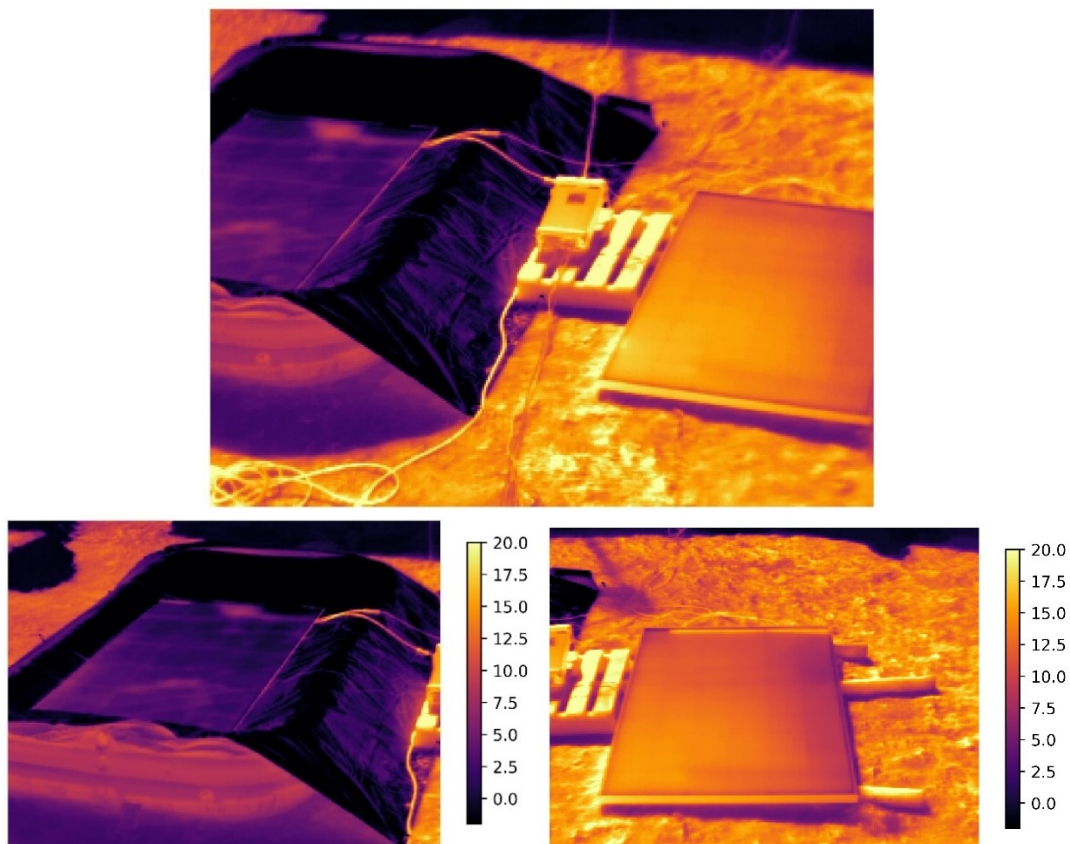


Figure 4.7: Top: IR picture of both modules. Bottom left: The floating module with some heat spots. Bottom right: The reference module.

4.1.3 U-value

Figure 4.8 illustrates the U-values for Tuesday 10.04 and Thursday 12.04. It is evident that the U-value for the reference module is rather stable throughout the test intervals for both days. The U-value for the floating module fluctuates more, while overall decreasing.

On Thursday, the temperature of the floating module was lower than the ambient until approximately 12.15 (see Figure 4.3). This gives a largely negative U-value. Thus, the time interval for the bottom graph was limited to avoid these values. Once the module temperature is higher than the ambient, the U-value becomes very large, due to the small temperature difference. After some time, both the temperature difference and the U-value become more stable.

By comparing the U-values from the two test days, it is indicated that the cooling effect is higher on Thursday 12.04. This is likely related to the higher ambient temperature and irradiance.

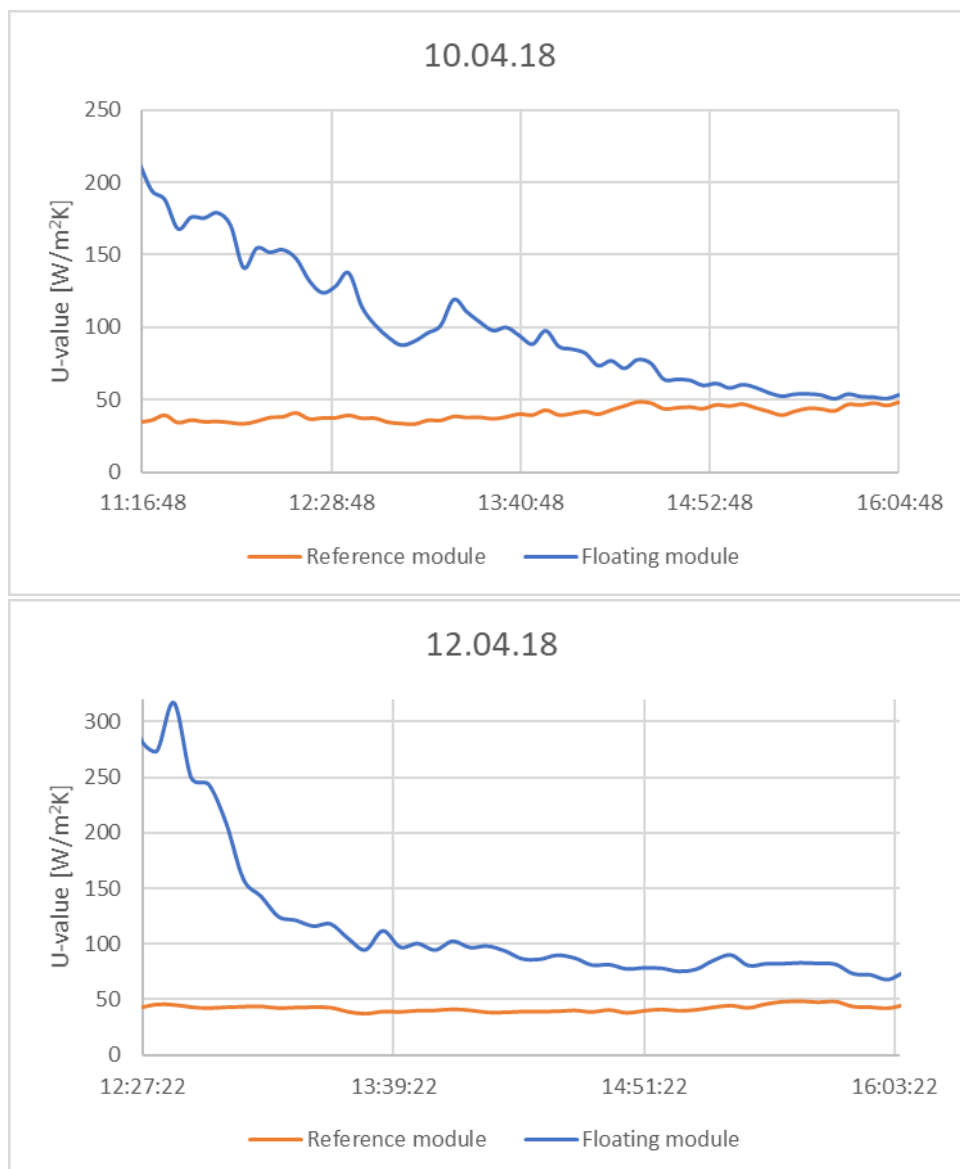


Figure 4.8: The U-value for the reference module and the floating module. The figure illustrates more stable conditions for the reference, and more fluctuating for the floating module. Top: Tuesday 10.04. Bottom: Thursday 12.04.

The cell temperature is estimated from equation 6, based on the measured back-surface temperature.

$$T_c = T_m + \frac{I_L}{I_{L0}} \Delta T \quad (6)$$

As seen previously in the chapter, the reference module temperature follows the behavior of the ambient temperature more closely than the floating module. The U-value is dependent upon the difference between cell temperature and ambient temperature, which leads to a stable reference U-value, while a more unstable floating U-value. The table below summarizes the average U-values for both modules.

Table 4.3: Summary of average U-value for both modules on Tuesday 10.04 and Thursday 12.04. The values are given as an average between 11.15 and 16.00, if not otherwise specified.

Average U-value	Reference module	Floating module
10.04.18	40.47	100.1
12.04.18	42.11	109.9 (12.30 – 16.00)

It may be argued that the U-value for the floating module is unstable as it highly depends on the temperature difference between the cell and the ambient. Temperature measurements conducted over a longer period would be beneficial to get a better and broader view of the U-value. Furthermore, the temperature measurements conducted at the test site have a degree of uncertainty, which in turn leads to uncertainty related to the U-values. However, the uncertainties are somewhat equal for each module, as the same equipment and methods are used, ultimately reducing the net error, when comparing the two modules.

For floating installations at other locations, where the temperature is higher during the day, the overall temperature of the PV module is likely to be more stable, mainly due to the water’s heat capacity. Because of this characteristic behavior, a floating module is likely to have fluctuating U-values.

To study how unconventional cooling of PV modules can be implemented in two relevant modeling software tools, PVsyst and TRNSYS, measurements from Tuesday 10.04 is used as a test case. This day provided the measurements with the least fluctuations. Thus, the U-value used for the simulations is 40.5 W/m²K for the reference simulations and 100 W/m²K for the floating simulations

4.1.4 Summary

It is indicated that the floating module has approximately 2-6 % higher normalized power output than the reference module for the test site at Kjeller. This difference is likely to be higher for other locations, as the test relies on a floating module placed in an inflatable pool, with stationary water.

The canvas used in the experiment at IFE is not applicable for an offshore installation. Ocean Sun’s canvas is thicker than the tarp and will not conduct heat as well. However, for an installation at sea, the ocean will arguably contribute to more effective cooling compared to stationary water in a pool. Thus, more results from the experiment in Singapore will be fundamental for the study on the cooling effect for modules in thermal contact with water.

The floating module has on average a lower back-surface temperature than the reference module, with an average difference of 5.92°C on Tuesday 10.04 and 7.45°C on Thursday 12.04. However, the measurements may overestimate the module temperatures, as the area under the temperature sensor is not cooled as effectively as the rest of the module. The pictures taken with the IR camera indicate a temperature difference in favor of the floating module, but also illustrate the warm spots.

The cooling effect for the reference module ranges around 40-50 W/m²K for the two test days with temperature sensors, which is higher than the values indicated by the theory. This might be due to the very good conditions at the test site; relatively low ambient temperature and high irradiance. The cooling effect for the floating module fluctuates more, making it difficult to set an exact value. However, the results indicate a U-value ranging between approximately 60-110 W/m²K, depending on the ambient and module temperatures.

Furthermore, the results indicate that the cooling effect increases when the ambient temperature and irradiance increase, as seen for Thursday 12.04. Naturally, an extended period of measurements, preferably under warmer, higher irradiance conditions, would be highly beneficial. Additionally, synchronizing the power output, irradiance and temperature logging from the test site at Kjeller might provide more exact measurements and calculation related to the cooling effect.

The module performance does not directly depend on the cooling effect, but rather on the operational temperature of the module. Thus, at higher U-values, the relative operating temperature will decrease, consequently leading to a higher relative performance. This arguably makes FPV a viable technology, as more power can be produced at the same area as for a terrestrial installation, or less area is needed to produce the same amount as from a terrestrial installation. However, the viability depends on the costs related to FPV, such as the LCOE. There is much uncertainty related to costs, as argued in chapter 2.5.2. Providing a cost estimate is outside the scope of this thesis, but it is highly recommended to investigate this for further work.

4.2 Estimated results from the thermal model

As discussed in chapter 3.4, calculating the correct heat transfer coefficient is very complex. Furthermore, calculating the correct thermal resistances for a real test site is also challenging, and several assumptions must be made.

Various parameter values were tested, aimed at being realistic while giving estimates close to the actual measurements.

Based on the discussion in chapter 3.4, the heat transfer coefficient for water is reduced to 300 W/m²K. Additionally, for the floating module, the overall thermal resistance for the back-side is increased and thus set equal to 0.0093 K/W. For the front side convection, equation 33 is used, and the wind speed is set equal to 1 m/s. Thus, the heat transfer coefficient for wind is 11.11 W/m²K, which according to theory is a probable value for a site with little wind. The water temperature is assumed to be constant and equal to 4°C. For the reference module's back side convection, the thermal resistance is set to 20 % of the front side, due to less air circulation than in the front.

Figure 4.9 illustrates the power output estimated from the thermal model, together with the actual power output measured at the test site. It is evident that the estimate is lower for both modules, but it is also indicated that the estimated power output of the floating module is higher than that of the reference module. The estimated power output from the reference module is on average 14.97 % lower than measured, and the estimated power output from the floating module is on average 17.32 % lower than measured, as illustrated in Table 4.4.

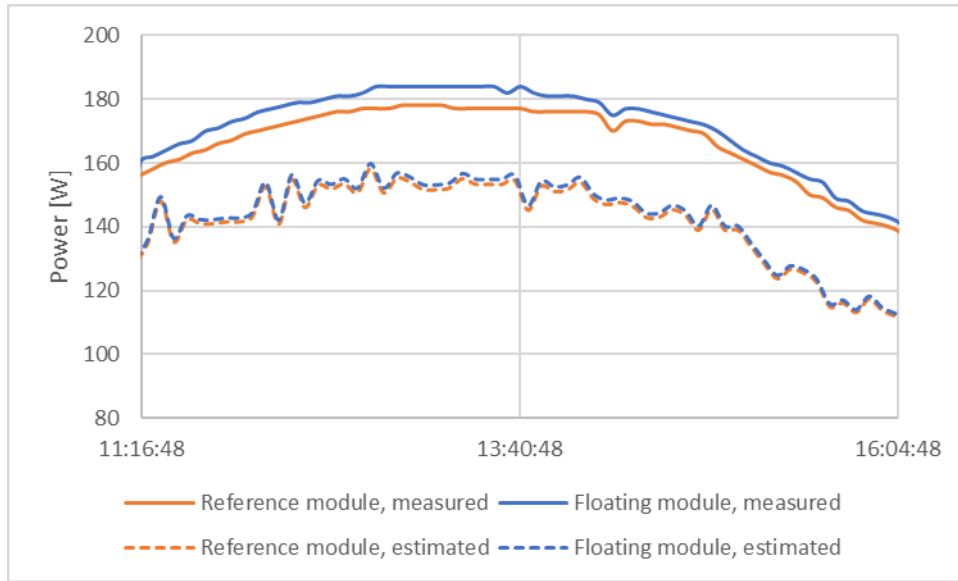


Figure 4.9: Illustration of estimated power output from both modules and measured power outputs from the test site at Kjeller.

Table 4.4: Average, maximum and minimum difference, in percentage, between measured and estimated power output for both modules.

Tuesday 10.04.18	Reference module	Floating module
Average difference [%]	14.97	17.32
Maximum difference [%]	21.26	22.84
Minimum difference [%]	7.39	9.65

It is clear that the thermal model underestimates the performance of both modules, especially for the floating module. The estimated average difference between the performance of the floating and the reference module is 0.90 %, which is quite lower than the actual difference.

Figure 4.10 illustrates the estimated cell temperature, as well as the cell temperatures derived from the measured back-surface temperatures. The results indicate that the temperature estimation is incorrect, as the estimated module temperatures are lower than the ambient temperature.

The average cell temperature, derived from the measured back-surface temperature, is 22.6°C for the reference module and 16.8°C for the floating module. The estimated average cell temperature from the thermal model is 13.2°C for the reference module and 10.9°C for the floating module. These are also below the average ambient temperature.

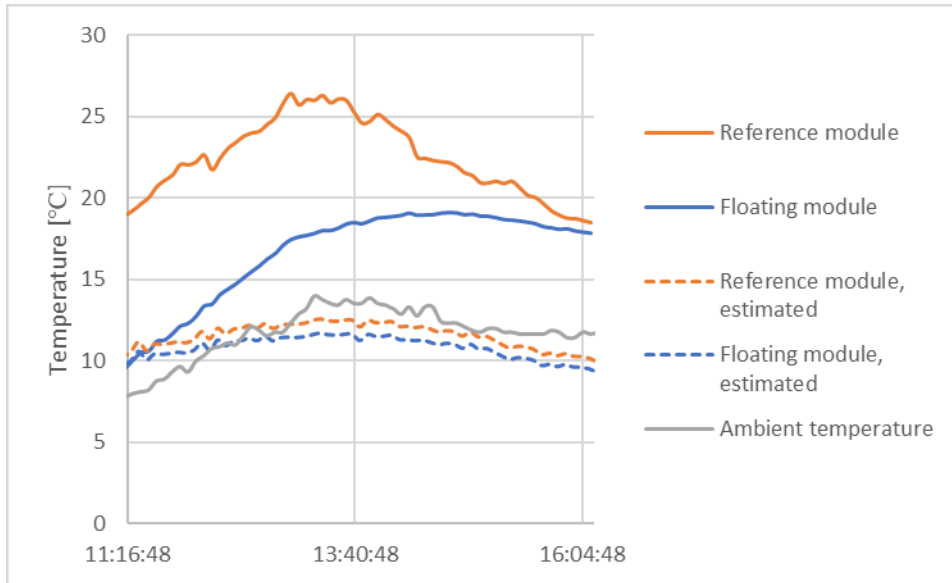


Figure 4.10: Comparison of cell temperatures estimated by the thermal model and cell temperatures derived from measurements of the back-surface temperature of the modules.

Thus, the thermal model does not estimate module temperatures satisfyingly. This is likely due to the simplicity of the model, in which heat capacities are not included. However, the model does estimate that the reference module temperature is higher than the floating module temperature, which is essentially correct, according to both theory and measurements.

Lower cell temperature than ambient temperature during the test interval is contradictory to the measurements conducted at the test site. Furthermore, it is contradictory to theory, according to equation 7, which argues that the cell temperature is higher than ambient temperature, depending on irradiance. In addition, cell temperatures below the ambient temperature leads to negative U-values, which also is contradictory to the measurements.

Figure 4.11 illustrates the estimated module efficiency, the measured module efficiency and the efficiency at STC. It is evident that the thermal model estimates an efficiency below the experimental efficiency, but also higher than the efficiency at STC, which is expected due to high irradiance and low ambient temperature. The efficiency from the thermal model is calculated from equation 31, which depends on the efficiency and temperature at STC, solar irradiance, thermal resistances and water temperature. Because the model does not incorporate heat capacities, and because the estimated cell temperature is rather constant, the estimated efficiency is in turn rather constant.

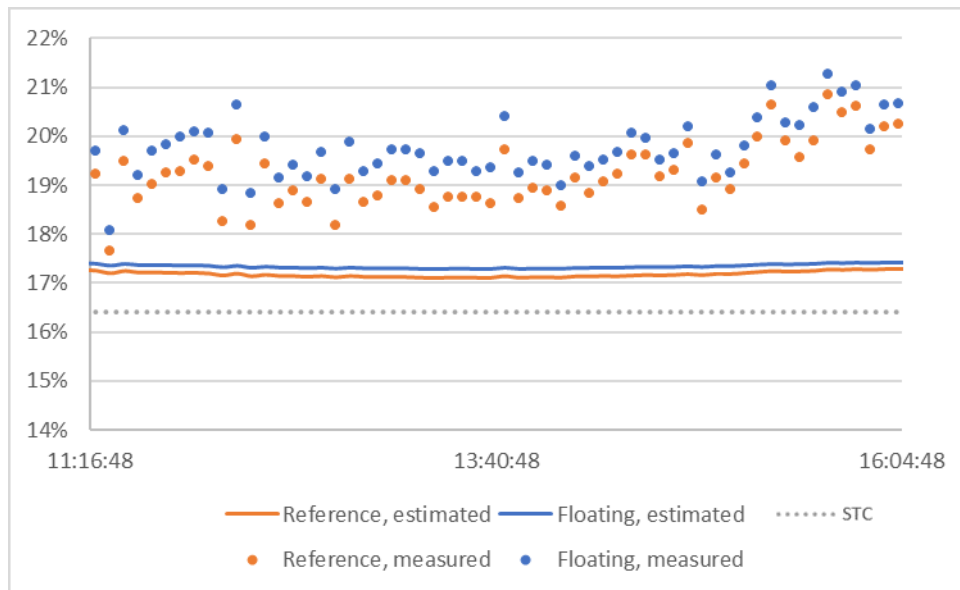


Figure 4.11: Illustration of estimated module efficiencies, measured module efficiencies and STC efficiency. The efficiency at STC is provided by the module's datasheet.

The thermal model can to some extent estimate the power outputs, and gives higher power output for a floating module compared to a reference module. However, if the model parameters are unknown or uncertain, large errors might occur. The more uncertainty there is related to the parameters, the more uncertainty will be related to the estimates from the model.

There are arguably several reasons for why the thermal model performs poorly. Not including heat capacities and time lagging is assumed to be the biggest cause for errors and inaccuracies. The model assumes that the irradiance which is not converted into electricity, gets lost as heat right away. This is highly unlikely, as energy will be stored in the PV modules, causing the temperature to rise. In addition, the parameters, as introduced in above, is likely to be inaccurate. There will also be significant uncertainties related to the irradiance measurements, and in this model, that will directly affect the difference between the modelled and measured temperature.

For further development of thermal models for floating PV installations, it is recommended to include heat capacities, time lagging, and investigate the parameters more carefully.

4.3 Results from computer simulations

The U-value used in the simulations is 40.5 W/m²K for the reference module and 100.1 W/m²K for the floating module. All simulations are studied in detail for the defined test interval; 11.15 – 16.00.

4.3.1 PV_{sys}

The simulated power output for the reference module and the floating module is illustrated in Figure 4.12 together with measured power outputs.

The simulated floating module performs on average 2.10 % better than the simulated reference module. This indicates that the software is capable of simulating different power outputs when U-values are given. However, the simulated improvement is lower than the actual improvement. The difference between the measured and the simulated power output is approximately 25 % for both modules, based

on normalized power output. The normalized power output for the simulation does not account for the internal differences apparent in the two modules used at the test site.

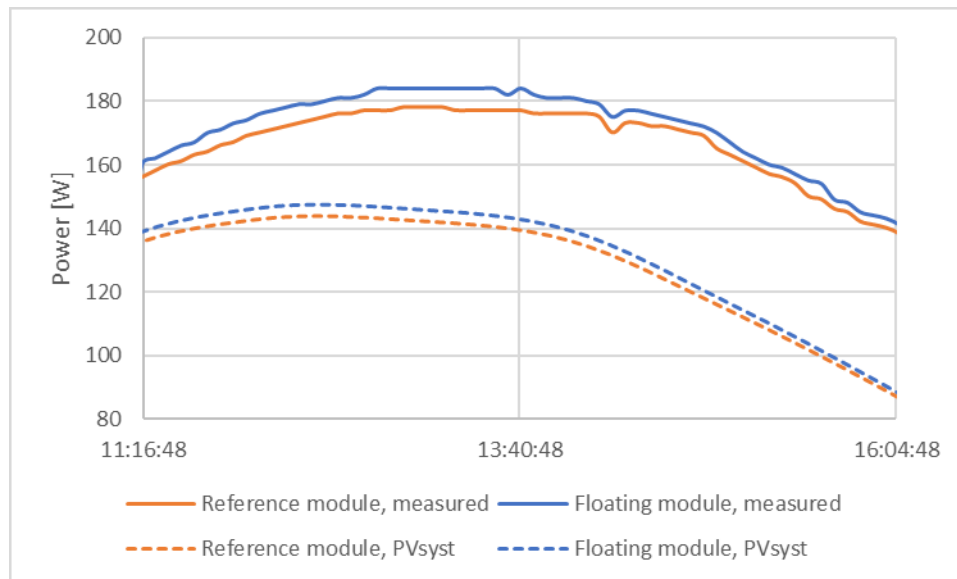


Figure 4.12: Simulated power output for the reference module and floating module, as well as measured power output from both modules at Kjeller.

Figure 4.13 illustrates the simulated cell temperatures for the reference module and the floating module, and the estimated cell temperatures derived from back-surface module temperatures. It is indicated in the figure that the simulated cell temperature for the reference module follows the behavior of the experimental cell temperature nicely. The simulated reference temperature is somewhat underestimated, by 1.32°C on average.

The simulated cell temperature for the floating module is on average 1.35°C lower than the experimental temperature. It starts out by being higher than the experimental temperature, but decreases more rapidly during the rest of the interval. It is clear that the simulated temperature for the floating module follows the behavior of the reference module. This is arguably because the heat capacity of water is not considered in the simulation.

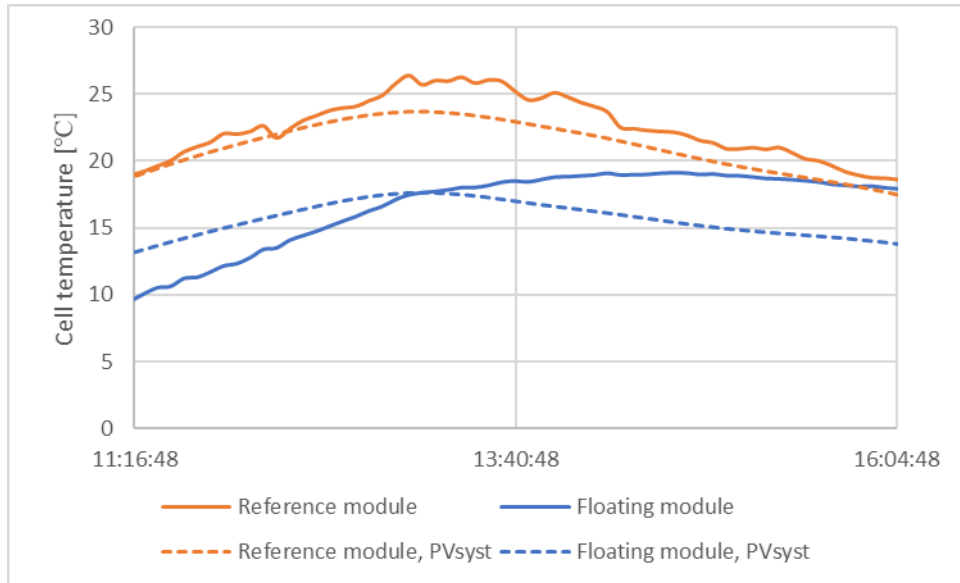


Figure 4.13: Simulated cell temperatures for both modules, and actual cell temperatures estimated from back-surface module temperature.

The average simulated temperature difference between the reference module and the floating module is 5.30 °C, which suggests that the change in effect should be 2.12 % on average, based on the temperature coefficient for P_{MPP} . This coincides with the difference in performance, as presented above.

4.3.2 TRNSYS

As explained by subchapter 3.5.2, the variable parameter for the TRNSYS simulations is wind speed. A wind speed of 1.92 m/s gives a U-value of 40.5 W/m²K, while a wind speed of 6.96 m/s gives a U-value of 100.1 W/m²K. Thus, these wind speeds are used for the reference simulation and floating simulation, respectively. Additionally, a simulation without wind speed was run.

Figure 4.14 illustrates the power outputs for all three simulations and the measured power output from the reference and floating module. It is evident that the simulations provide power outputs lower than measured power output.

For the reference simulation which includes wind, the power output is on average 23.0 % lower than the experimental results. However, there is an improvement in simulated power output when the wind speed is included, compared to when it is not included. This is expected.

The simulated power output for the floating module is on average 23.7 % lower than the measured power output for the defined test interval. Furthermore, the simulated power output for the floating module is 2.22 % higher than the reference simulation without wind, and 0.69 % higher than the reference simulation with wind.

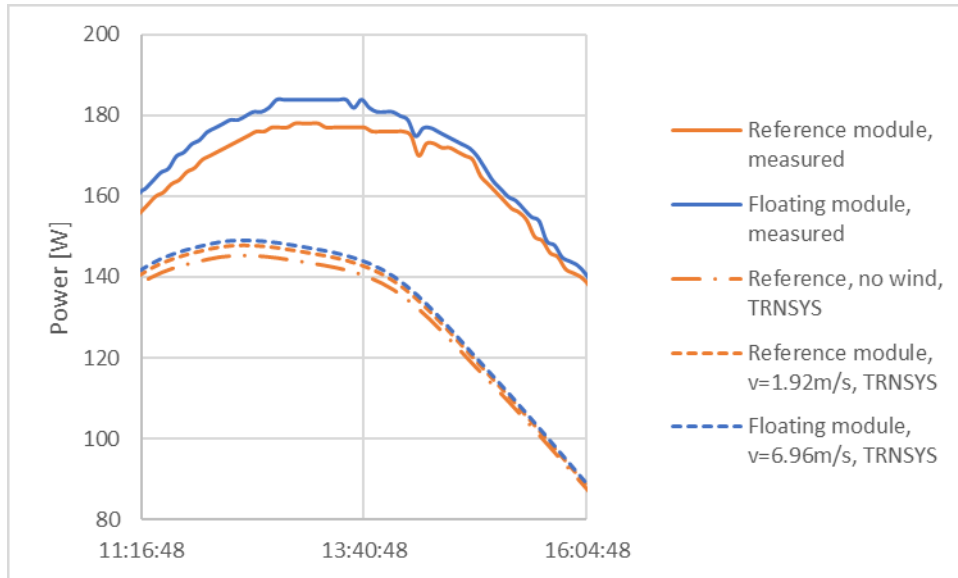


Figure 4.14: Simulated power outputs from TRNSYS. For the reference module, one simulation without wind as a parameter and one simulation where wind speed is set to 1.92 m/s is included. The simulation for the floating module takes wind speed equal to 6.96 m/s. Measured power from both modules is included.

Figure 4.15 illustrates the simulated cell temperatures and the cell temperatures derived from measured back-surface temperature.

For the reference module, the results indicate that simulated temperatures are lower than the experimental temperature. Even when there is no wind included in the simulation, the reference temperature is too low compared to the cell temperature derived from the measurements. The temperature difference between the experimental temperature and the simulated temperature (with wind) is on average 7.47°C.

For the floating module, the simulated cell temperature is on average 3.80°C lower than the experimental temperature. The results indicate that the simulated cell temperature is somewhat higher than the estimated cell temperature in the beginning of the time interval, while it decreases too rapidly during the rest of the time interval. It is also evident that the simulation of floating PV module temperatures is incorrect, arguably because of the heat capacity of water, which is not considered, as it is not a feature in TRNSYS. Regardless, the simulation provides lower module temperature than measured, which should imply higher power output than measured.

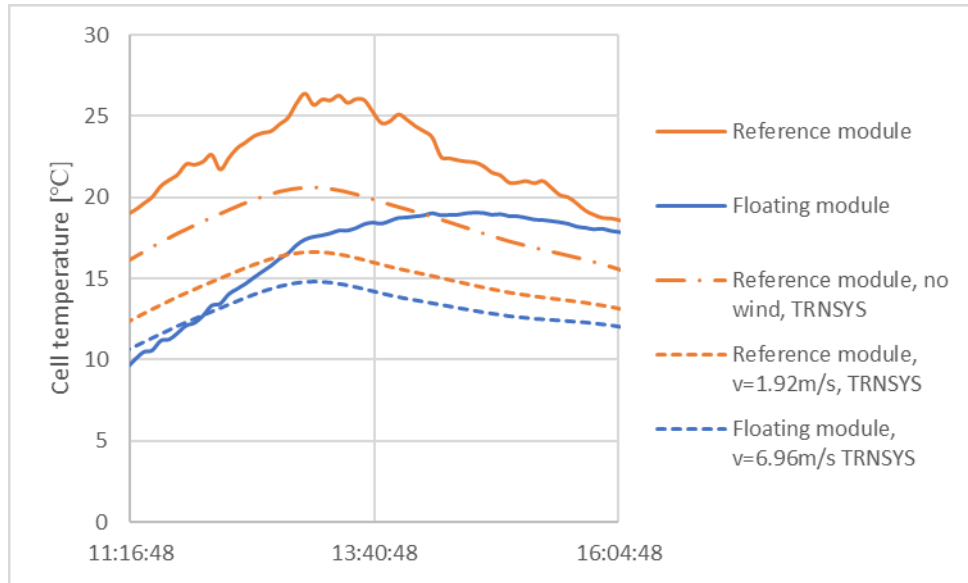


Figure 4.15: Simulated cell temperatures and cell temperatures derived from measured back-surface temperature. For the reference module, one simulation without wind as a parameter and one simulation where wind speed is set to 1.92 m/s is included. The simulation for the floating module takes wind speed equal to 6.96 m/s.

The average simulated temperature difference between the reference module (with wind) and the floating module is 1.61°C, which suggests that the change in effect should be 0.64 % based on the temperature coefficient for P_{MPP} . This coincides quite well with the simulated difference in power output.

4.3.3 Comparison of simulated and experimental results

Table 4.5 compares and summarizes the simulated results with the experimental results. Both PVsyst and TRNSYS underestimate the power production for both modules, compared to the actual output, by approximately 23-25 %. Furthermore, both simulation programs underestimate the cell temperatures.

Table 4.5: Summary of power output and temperature differences from the simulations, compared to experimental results. Every value is given as an average for the defined test interval. Only the reference simulation with wind is included, because that is the simulation which operate with the correct U-value.

	Reference module		Floating module	
	PVsyst	TRNSYS (wind)	PVsyst	TRNSYS
Difference from measurements				
Power output	-25 %	-23.0 %	-25 %	-23.7 %
Temperature [°C]	-1.32	-7.47	-1.35	-3.80

Figure 4.16 summarizes and compares the module efficiencies from the simulations and the experiment, and STC efficiency. The figure illustrates how the experimental modules have higher efficiency than STC efficiency, while the software programs simulate lower efficiencies. It is also clear that TRNSYS provides higher module efficiency than PVsyst. As the loggings of power output and solar irradiance were not synchronized at the test site, the experimental module efficiencies calculated might be somewhat incorrect. Regardless, the experimental efficiency is higher than the STC efficiency.

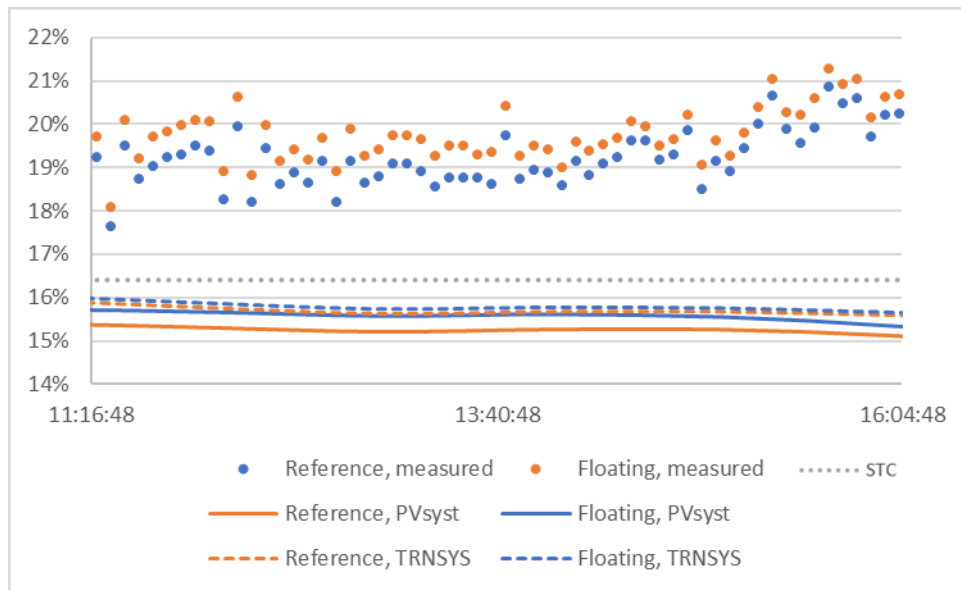


Figure 4.16: Efficiencies for both modules; measured from test site and simulated from PVsyst and TRNSYS. The efficiency at STC given by the datasheet is illustrated by the dotted gray line. The experimental results are plotted with five-minute intervals, while the simulated values are plotted with hourly intervals.

As discussed, both simulation programs underestimate power output. The difference might be explained by the very good conditions at the test site, which neither PVsyst nor TRNSYS seem to incorporate well enough in the simulations. The difference might also be explained by inaccuracies in the data input, such as solar irradiance and ambient temperature. Every simulation was given the same inputs, so the initial differences for each simulation have the same uncertainties or errors. This might explain why the programs simulate rather equal power outputs. However, to test this further, extended measurements for the test site at Kjeller and other test sites would be beneficial. Optimally, results from the test site at Singapore would have been used for this purpose.

For TRNSYS, there might be some simulation errors related to the inverter, in which it is either overestimated or underestimated. If so, there will be equal errors for each module. However, given that the results from PVsyst and TRNSYS do not differ by much, there is reason to believe that there are other sources of errors, as explained above.

For TRNSYS, the results indicate that increasing the wind speed improves the performance of PV modules, and that it might be used to manipulate FPV results. However, the simulated power outputs are significantly lower than the measured outputs. Arguably, this is not due to the wind speed variable, as it is evident that increasing wind speed increases the power output, but not by the amount that defines the difference. Thus, the wind speed is not assumed to be the reason behind the underestimation of power output.

Similarly, for PVsyst, it is not assumed that the *thermal parameter* is causing the significant difference in power output. Manually creating the 270W REC Peak Energy module might have led to some inaccuracies. However, the simulation was checked against a simulation with the 265W REC PE, which gave similar, but somewhat lower results, which is expected.

While both simulation programs underestimate the cell temperatures, PVsyst seem to simulate more accurately compared to TRNSYS. It should be noted that there are some uncertainties related to the actual cell temperatures, as it is derived from the measured back-surface temperatures. The actual cell temperatures might be lower than indicated in the figures, thus leading to a smaller difference with the

simulated results. Regardless of this, an underestimation for cell temperatures should lead to higher power outputs, according to theory. This is contradicting to the results.

In TRNSYS, the simulation which does not include wind speed shows that TRNSYS underestimates the cell temperature regardless, based on the experimental results from Kjeller.

As discussed in chapter 4.1.2, the cell temperature for the floating module depends on the heat capacity of water, and responds more slowly to changes in ambient temperature, compared to the reference module. Thus, including heat capacities for the surrounding materials in the simulations might lead to more correct cell temperatures for the floating module. However, if the heat capacity of water had been included in these simulations, the floating cell temperatures should have been higher, leading to lower power output at the end of the time interval.

The wind speed values given in the inputs for PVsyst is based on average values from Kjeller Airport, a location in which wind speed is arguably higher than at the test site. Including more detailed and specific measurements of wind speed for the test site as an input might lead to different results. As it is likely that the actual wind speed is lower than simulated, according to theory, the power outputs should decrease and the cell temperatures increase.

Furthermore, it would be beneficial to include wind speed measured at a specific test site for simulations run in TRNSYS, instead of using it to manipulate answers for FPV. Thus, for future modeling features in TRNSYS, including a thermal coefficient given as a parameter is suggested.

It is suggested to expand the features of the software programs to include installations at water bodies. This might be done by including water temperature, heat capacities and other thermal properties. It is also suggested to conduct more measurements and experiments similar to the work done in this thesis, to extend the results and interpretations of results.

5 Conclusions

For the test site at IFE and the test period considered, the floating module in thermal contact with water had approximately 2-6 % higher normalized power output than the reference module. Furthermore, the floating module had lower back-surface temperature than the reference module during the test intervals. The temperature difference increased at higher ambient temperatures and was on average 5.9°C on Tuesday 10.04.18 and 7.5°C on Thursday 12.04.18. Additionally, IR pictures taken of the modules proved a significant temperature difference in favor of the floating module.

The preliminary results from the test site in Singapore also suggests that floating modules in thermal contact with water will have higher performance and lower operational temperatures compared to modules without thermal contact with water.

The cooling effect for the reference module was quite stable throughout the test intervals, ranging between 40-50 W/m²K, while the cooling effect for the floating module was more fluctuating. The results indicate that the U-value for the floating module ranges between approximately 60-110 W/m²K, depending on the ambient and module temperatures.

The thermal model underestimated the power outputs from both modules, but estimated a higher power output for the floating module compared to the reference module, based on data from the test site. The model did not estimate module temperatures correctly. For the modeling of floating PV, it has become clear that the heat capacity of water must be included, as it affects the behavior of the module.

Both PVsyst and TRNSYS underestimated the power outputs compared to the experimental power outputs. This was arguably caused by other reasons than the cooling effect, which was used as input in the simulations. Both programs provided simulations with higher power outputs for the floating module compared to the reference module. Additionally, PVsyst simulated cell temperatures more correctly than TRNSYS. So far, PVsyst seems to be the software best suited for simulating floating PV, as the thermal losses can be adjusted for increased cooling effect due to the thermal contact with water.

As FPV is a technology on the rise, the demand for modeling such installations is likely to increase. So far, neither PVsyst nor TRNSYS have features for modeling the technology. Thus, it is recommended that the software programs are developed to include such features, by including heat capacities of materials surrounding the installations and making water surfaces available as sites. For further experimental testing and modeling of floating PV modules, it is recommended to investigate and develop suitable materials and installation solutions.

6 Further work

As the FPV technology is relatively new and growing, there are many objectives relevant for further investigation. Based on the work in this thesis, some suggestions include:

- Evaluate and analyze experimental results from an FPV installation over a longer time period for relevant locations.
- Develop features in software programs to model FPV. This may include features such as heat capacities, water temperature and making water bodies available as sites.
- Develop (3D) thermal models for FPV, which respond to water surfaces in terms of heat capacities and time lagging effects.
- Evaluate different PV technologies for offshore FPV installations. Other technologies might be more suitable for offshore installations due to more flexible structures and more resistance towards harsher weather conditions.
- Evaluate costs of a (offshore) floating installation.
- Evaluate the risks of floating solar PV, in terms of electrical and mechanical issues due to harsher weather conditions.
- Quantify the soiling effect from salt water on offshore horizontal modules and how it affects the performance of floating modules.
- Evaluate the degradation for floating modules, such as microcracks due to harsher weather conditions for offshore FPV.
- Investigate the coupling effect between FPV and hydropower.

References

- Afework, B., G., L., Hanania, J. & Donev, J. (2018). *Levelized cost of energy*: Energy Education. Available at: http://energyeducation.ca/encyclopedia/Levelized_cost_of_energy (accessed: 14.03.2018).
- APsystems. (2016). *APsystems YC500I microinverter datasheet*. Available at: https://emea.apsystems.com/wp-content/uploads/2018/04/APsystems-YC500I-EU_09_2016.pdf (accessed: 20.04.2018).
- Armstrong, S. & Hurley, W. (2010). A thermal model for photovoltaic panels under varying atmospheric conditions. *Applied Thermal Engineering*, 30 (11-12): 1488-1495.
- Azmi, M. S. M., Othman, M. Y. H., Ruslan, M. H. H., Sopian, K. & Majid, Z. A. A. (2013). Study on electrical power output of floating photovoltaic and conventional photovoltaic. 95-101. doi: 10.1063/1.4858636.
- Bahaidarah, H., Subhan, A., Gandhidasan, P. & Rehman, S. (2013). Performance evaluation of a PV (photovoltaic) module by back surface water cooling for hot climatic conditions. *Energy*, 59: 445-453. doi: 10.1016/j.energy.2013.07.050.
- Bejan, A. & Kraus, A. D. (2003). *Heat transfer handbook*, vol. 1. New York: John Wiley & Sons.
- Bellini, E. (2018). *Dutch consortium plans world's first "off-shore" floating PV plant for the North Sea*. Available at: <https://www.pv-magazine.com/2018/02/07/dutch-consortium-plans-worlds-first-off-shore-floating-pv-plant-for-the-north-sea/> (accessed: 19.03.2018).
- Bergman, T. L., Incropera, F. P., DeWitt, D. P. & Lavine, A. S. (2011). *Fundamentals of heat and mass transfer*. New York: John Wiley & Sons.
- Brandon, S. (2017). *China just switched on the world's largest floating solar power plant*. Available at: <https://www.weforum.org/agenda/2017/06/china-worlds-largest-floating-solar-power/> (accessed: 19.03.2018).
- Choi, Y.-K. (2014). A Study on Power Generation Analysis of Floating PV System Considering Environmental Impact. *International Journal of Software Engineering and Its Applications*, 8 (1): 75-84. doi: 10.14257/ijseia.2014.8.1.07.
- Dash, P. K. & Gupta, N. C. (2015). Effect of Temperature on Power Output from Different Commercially available Photovoltaic Modules. *International Journal of Engineering Research and Applications*, 5 (1): 148-151.
- Denny, M. W. (1993). *Air and water: the biology and physics of life's media*. New Jersey: Princeton University Press.
- F-Chart Software. (2018). *Engineering Equation Solver - Overview*. Available at: <http://www.fchart.com/ees/> (accessed: 17.04.2018).
- Ferrer-Gisbert, C., Ferrán-Gozálvez, J. J., Redón-Santafé, M., Ferrer-Gisbert, P., Sánchez-Romero, F. J. & Torregrosa-Soler, J. B. (2013). A new photovoltaic floating cover system for water reservoirs. *Renewable energy*, 60: 63-70.
- FLIR Systems. (2014). *FLIR A325sc datasheet*. Available at: http://www.flirmedia.com/MMC/THG/Brochures/RND_010/RND_010_US.pdf (accessed: 20.04.2018).

- Graham, S., Parkinson, C. & Chahine, M. (2010). *The Water Cycle*. NASA Earth Observatory. Available at: <https://earthobservatory.nasa.gov/Features/Water/> (accessed: 02.05.2018).
- Greene, W., Skorge, L. & Thorud, B. (2016). *Ocean Sun Offshore Floating PV Systems: Global Market & Commercial Performance Study*. Unpublished manuscript.
- Harvey, F. (2016). *World's biggest floating solar farm powers up outside London*. Available at: <https://www.theguardian.com/environment/2016/feb/29/worlds-biggest-floating-solar-farm-power-up-outside-london> (accessed: 19.03.2018).
- Honsberg, C. & Bowden, S. (2013). *PVeducation.org*. Available at: <http://www.pveducation.org/> (accessed: 08.03.2018).
- IEA. (2017). *Key world statistics*. Available at: <http://www.iea.org/publications/freepublications/publication/KeyWorld2017.pdf> (accessed: 03.05.2018).
- IEA. (2018). *International Energy Agency - Climate Change*. Available at: <https://www.iea.org/topics/climatechange/> (accessed: 02.05.2018).
- Ingenieurbüro Mencke & Tegtmeyer GmbH. (2016). *Silicon irradiance sensor datasheet*. Available at: https://www.imt-solar.com/fileadmin/docs/en/products/Si-Sensor_E.pdf (accessed: 19.04.2018).
- Ingenieurbüro Mencke & Tegtmeyer GmbH. (2018). *Ta-V-4090 datasheet*. Available at: <https://www.imt-solar.com/products/temperature-sensor/ambient-temperature/> (accessed: 19.04.2018).
- JRC EC. (2017). *Photovoltaic Geographical Information System - Interactive Tools - Monthly Irradiation Data*. Available at: http://re.jrc.ec.europa.eu/pvg_tools/en/tools.html#MR (accessed: 24.04.2018).
- Kratochvil, J. A., Boyson, W. E. & King, D. L. (2004). *Photovoltaic array performance model*: Sandia National Laboratories.
- Liu, L., Wang, Q., Lin, H., Li, H., Sun, Q. & wannersten, R. (2017). Power Generation Efficiency and Prospects of Floating Photovoltaic Systems. *Energy Procedia*, 105: 1136-1142. doi: 10.1016/j.egypro.2017.03.483.
- Løvik, H. (2017). *Satser på storskala flytende solceller*. Available at: <https://www.tu.no/artikler/satser-pa-storskala-flytende-solceller/411295> (accessed: 26.02.2018).
- Mesbahi, M. & Minamino, S. (2018). *Top 70 Floating Solar PV Plants*. Available at: <https://www.solarplaza.com/channels/top-10s/11761/top-70-floating-solar-pv-plants/> (accessed: 19.03.2018).
- Ocean Sun. (2017). *Ocean Sun - About*. Available at: <http://oceansun.no/about/> (accessed: 24.02.2018).
- PVsys SA. (2012). *About us - Our objectives*. Available at: <http://www.pvsyst.com/en/about-us/our-objectives> (accessed: 20.03.2018).

- PVsyst SA. (2017). *PVsyst's forum* Available at: <http://forum.pvsyst.com/viewtopic.php?f=29&t=3025&p=7722&hilit=albedo#p7722> (accessed: 12.02.2018).
- PVsyst SA. (2018). *PVsyst 6 Help (built-in software)*. Available at: <http://files.pvsyst.com/help/> (accessed: 13.03.2018).
- Reindl, T. (2018). At the heart of floating solar: Singapore. *Pv-Tech Power*, 14: 18-23.
- Sahu, A., Yadav, N. & Sudhakar, K. (2016). Floating photovoltaic power plant: A review. *Renewable and Sustainable Energy Reviews*, 66: 815-824. doi: 10.1016/j.rser.2016.08.051.
- Skoplaki, E. & Palyvos, J. A. (2009). On the temperature dependence of photovoltaic module electrical performance: A review of efficiency/power correlations. *Solar Energy*, 83 (5): 614-624. doi: 10.1016/j.solener.2008.10.008.
- Smets, A., Jäger, K., Isabella, O., Swaaij, R. V. & Zeman, M. (2016). *Solar Energy: The physics and engineering of photovoltaic conversion, technologies and systems*. Cambridge: UIT Cambridge.
- SolarEdge Technologies. (2014). *SolarEdge Control and Communication Gateway SE1000-CCG-G datasheet*. Available at: https://www.solaredge.com/sites/default/files/se_control_and_communication_gateway.pdf (accessed: 26.04.2018).
- The Engineering ToolBox. *Plastics - Thermal conductivity of plastics*. Available at: https://www.engineeringtoolbox.com/thermal-conductivity-plastics-d_1786.html (accessed: 04.04.2018).
- Trapani, K. & Millar, D. L. (2014). The thin film flexible floating PV (T3F-PV) array: The concept and development of the prototype. *Renewable Energy*, 71: 43-50. doi: 10.1016/j.renene.2014.05.007.
- TRNSYS. (2018). *What is TRNSYS?* Available at: <http://www.trnsys.com/> (accessed: 20.02.2018).
- TRNSYS Technical Support Team. (2018). *Email correspondance with TRNSYS Technical Support Team*. Kjeller (27.02.2018).
- UNFCCC. (2018a). *Introduction to Mitigation*. Available at: <https://unfccc.int/topics/mitigation/the-big-picture/introduction-to-mitigation> (accessed: 02.05.2018).
- UNFCCC. (2018b). *The Paris Agreement*. Available at: <https://unfccc.int/process-and-meetings/the-paris-agreement/the-paris-agreement> (accessed: 02.05.2018).
- Været som var (detaljert) Kjeller Flyplass, Skedsmo (Akerhus)*. (2018). Available at: https://www.yr.no/sted/Norge/Akershus/Skedsmo/Kjeller_flyplass/detaljert_statistikk.html (accessed: 14.04.2018).
- World sea temperature. (2018). *Singapore Sea Temperature*. Available at: <https://www.seatemperature.org/asia/singapore/singapore.htm> (accessed: 26.02.2018).
- Zhou, J., Yi, Q., Wang, Y. & Ye, Z. (2015). Temperature distribution of photovoltaic module based on finite element simulation. *Solar Energy*, 111: 97-103. doi: 10.1016/j.solener.2014.10.040.

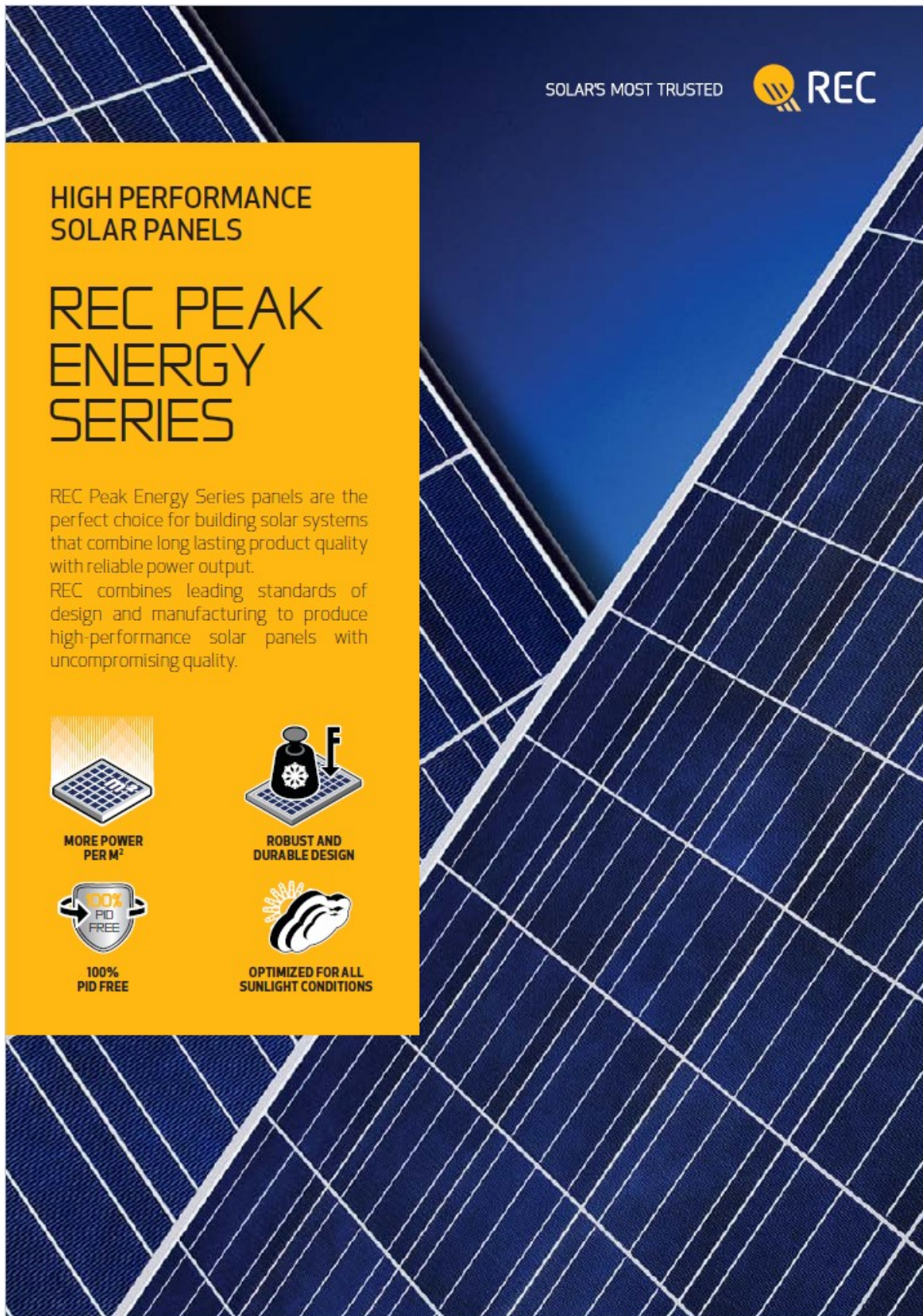
Appendix


Appendix A: Datasheet for modules

Appendix B: Sunburn Repeatability Results from the flash test

Appendix A

Electrical and mechanical specifications for the PV modules at the test site at IFE; REC270PE







SOLAR'S MOST TRUSTED 

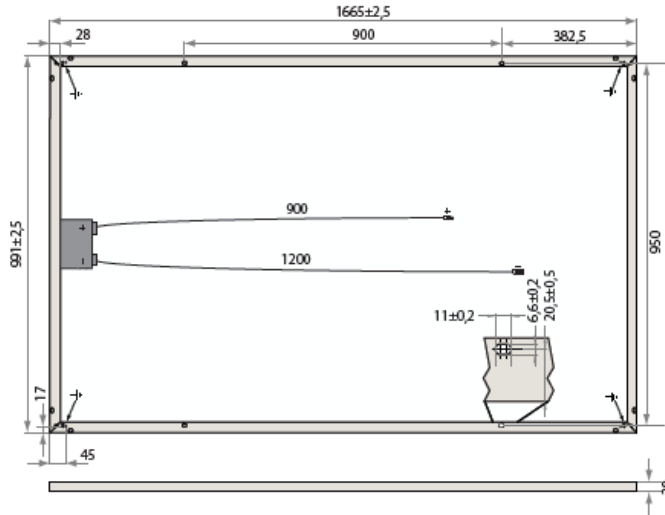
HIGH PERFORMANCE SOLAR PANELS

REC PEAK ENERGY SERIES

REC Peak Energy Series panels are the perfect choice for building solar systems that combine long lasting product quality with reliable power output. REC combines leading standards of design and manufacturing to produce high-performance solar panels with uncompromising quality.

- 
MORE POWER PER M²
- 
ROBUST AND DURABLE DESIGN
- 
100% PID FREE
- 
OPTIMIZED FOR ALL SUNLIGHT CONDITIONS

REC PEAK ENERGY SERIES



Measurements in mm [in]

ELECTRICAL DATA @ STC

Product Code*: RECxxxPE

	250	255	260	265	270	275
Nominal Power- P_{MPP} (Wp)	250	255	260	265	270	275
Watt Class Sorting - (W)	-0/+5	-0/+5	-0/+5	-0/+5	-0/+5	-0/+5
Nominal Power Voltage- V_{MPP} (V)	30.2	30.5	30.7	30.9	31.2	31.5
Nominal Power Current- I_{MPP} (A)	8.30	8.42	8.50	8.58	8.66	8.74
Open Circuit Voltage- V_{OC} (V)	37.4	37.6	37.8	38.1	38.4	38.7
Short Circuit Current- I_{SC} (A)	8.86	8.95	9.01	9.08	9.18	9.25
Panel Efficiency (%)	15.2	15.5	15.8	16.1	16.4	16.7

Values at standard test conditions (STC: air mass AM1.5, irradiance 1000 W/m², temperature 25°C), based on a production spread with a tolerance of V_{OC} & I_{SC} ±3% within one watt class. At low irradiance of 200 W/m² at least 95.5% of the STC module efficiency will be achieved.
*Where xxx indicates the nominal power class (P_{MPP}) at STC indicated above, and can be followed by the suffix BLK for black framed modules.

ELECTRICAL DATA @ NMOT

Product Code*: RECxxxPE

	183	187	190	193	196	202
Nominal Power- P_{MPP} (Wp)	183	187	190	193	196	202
Nominal Power Voltage- V_{MPP} (V)	27.8	28.0	28.2	28.4	28.6	28.8
Nominal Power Current- I_{MPP} (A)	6.58	6.68	6.74	6.80	6.86	7.02
Open Circuit Voltage- V_{OC} (V)	34.7	34.8	35.0	35.3	35.7	36.0
Short Circuit Current- I_{SC} (A)	7.11	7.18	7.23	7.29	7.35	7.40

Nominal module operating temperature (NMOT): air mass AM1.5, irradiance 800 W/m², temperature 20°C, wind speed 1 m/s.
*Where xxx indicates the nominal power class (P_{MPP}) at STC indicated above, and can be followed by the suffix BLK for black framed modules.

CERTIFICATIONS



takeaway take-e-way WEEE-compliant recycling scheme

WARRANTY

10 year product warranty
25 year linear power output warranty
(max. degradation in performance of 0.7% p.a.)
See warranty conditions for further details.

16.7% EFFICIENCY

10 YEAR PRODUCT WARRANTY

25 YEAR LINEAR POWER OUTPUT WARRANTY

GENERAL DATA

Cell type:	60 multicrystalline cells 3 strings of 20 cells in series
Glass:	3.2 mm solar glass with anti-reflection surface treatment
Backsheet:	Highly resistant polyester
Frame:	Anodized aluminum (silver / black)
Junction box:	3 bypass diodes, IP67 rated in accordance with IEC 62790
Cable:	4 mm ² solar cable, 0.9 m + 1.2 m in accordance with EN 50618
Connectors:	Stäubli MC4 PV-KBT4/PV-KST4 (4 mm ²) Tonglin TL-Cable 015-FR (4 mm ²) in accordance with IEC 62852, IP68 only when connected
Origin:	Made in Singapore

MAXIMUM RATINGS

Operational temperature:	-40 ... +85°C
Maximum system voltage:	1000 V
Design load (+): snow	367 kg/m ² (3600 Pa)*
Maximum test load (+):	550 kg/m ² (5400 Pa)
Design load (-): wind	163 kg/m ² (1600 Pa)*
Maximum test load (-):	244 kg/m ² (2400 Pa)
Max series fuse rating:	25 A
Max reverse current:	25 A

* Safety factor 1.5

TEMPERATURE RATINGS*

Nominal Module Operating Temperature:	45.7°C (±2°C)
Temperature coefficient of P_{MPP} :	-0.40 %/°C
Temperature coefficient of V_{OC} :	-0.27 %/°C
Temperature coefficient of I_{SC} :	0.024 %/°C

* The temperature coefficients stated are linear values

MECHANICAL DATA


Dimensions:	1665 x 991 x 38 mm
Area:	1.65 m ²
Weight:	18 kg

Specifications subject to change without notice. Ref: REC-05/057-01 Rev.-Z-08/17

Founded in Norway in 1996, REC is a leading vertically integrated solar energy company. Through integrated manufacturing from silicon to wafers, cells, high-quality panels and extending to solar solutions, REC provides the world with a reliable source of clean energy. REC's renowned product quality is supported by the lowest warranty claims rate in the industry. REC is a Bluestar Elkem company with headquarters in Norway and operational headquarters in Singapore. REC employs more than 2,000 people worldwide, producing 1.4 GW of solar panels annually.

REC
www.recgroup.com





SOLAR'S MOST TRUSTED 

REC TWINPEAK 2 SERIES

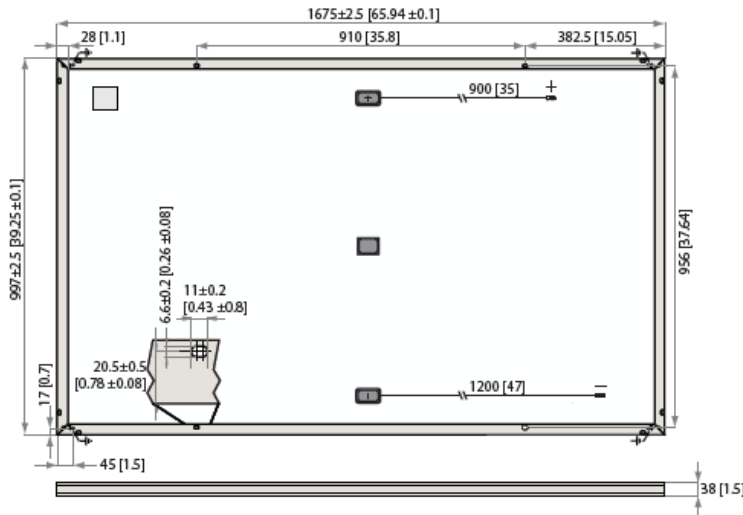
**PREMIUM SOLAR PANELS
WITH SUPERIOR PERFORMANCE**

REC TwinPeak 2 Series solar panels feature an innovative design with high panel efficiency and power output, enabling customers to get the most out of the space used for the installation.

Combined with industry-leading product quality and the reliability of a strong and established European brand, REC TwinPeak 2 panels are ideal for residential and commercial rooftops worldwide.

- 
**MORE POWER
OUTPUT PER M²**
- 
**IMPROVED PERFORMANCE
IN SHADED CONDITIONS**
- 
**100%
PID FREE**
- 
**REDUCES BALANCE OF
SYSTEM COSTS**

REC TWINPEAK 2 SERIES



Measurements in mm [in]

ELECTRICAL DATA @ STC

Product code*: RECxxxTP2

	275	280	285	290	295	300
Nominal Power- P_{MPP} (Wp)	275	280	285	290	295	300
Watt Class Sorting- (W)	-0/+5	-0/+5	-0/+5	-0/+5	-0/+5	-0/+5
Nominal Power Voltage- V_{MPP} (V)	31.5	31.7	31.9	32.1	32.3	32.5
Nominal Power Current- I_{MPP} (A)	8.74	8.84	8.95	9.05	9.14	9.24
Open Circuit Voltage- V_{OC} (V)	38.2	38.4	38.6	38.8	39.0	39.2
Short Circuit Current- I_{SC} (A)	9.52	9.61	9.66	9.71	9.76	9.82
Panel Efficiency (%)	16.5	16.8	17.1	17.4	17.7	18.0

Values at standard test conditions (STC: air mass AM1.5, irradiance 1000 W/m², temperature 25°C), based on a production spread with a tolerance of V_{OC} & I_{SC} ±3% within one watt class. At a low irradiance of 200 W/m² at least 95% of the STC module efficiency will be achieved.
*Where xxx indicates the nominal power class (P_{MPP}) at STC indicated above, and can be followed by the suffix BLK for black framed modules.

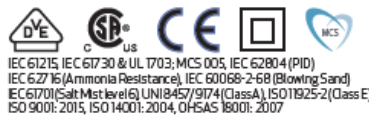
ELECTRICAL DATA @ NMOT

Product code*: RECxxxTP2

	206	210	214	218	223	226
Nominal Power- P_{MPP} (Wp)	206	210	214	218	223	226
Nominal Power Voltage- V_{MPP} (V)	29.2	29.4	29.6	29.8	30.0	30.1
Nominal Power Current- I_{MPP} (A)	7.07	7.15	7.24	7.32	7.43	7.51
Open Circuit Voltage- V_{OC} (V)	35.4	35.6	35.8	36.0	36.2	36.3
Short Circuit Current- I_{SC} (A)	7.52	7.59	7.68	7.75	7.85	7.91

Nominal module operating temperature (NMOT: air mass AM1.5, irradiance 800 W/m², temperature 20°C, wind speed 1 m/s).
*Where xxx indicates the nominal power class (P_{MPP}) at STC indicated above, and can be followed by the suffix BLK for black framed modules.

CERTIFICATIONS



takeaway take-e-way WEEE-compliant recycling scheme

WARRANTY

10 year product warranty
25 year linear power output warranty
(max. degradation in performance of 0.7% p.a.)
See warranty conditions for further details.

18.0% EFFICIENCY

10 YEAR PRODUCT WARRANTY

25 YEAR LINEAR POWER OUTPUT WARRANTY

GENERAL DATA

Cell type:	120 half-cut multicrystalline PERC cells 6 strings of 20 cells in series
Glass:	3.2 mm solar glass with anti-reflection surface treatment
Backsheet:	Highly resistant polyester polyolefin construction
Frame:	Anodized aluminum (silver / black)
Junction box:	3-part, 3 bypass diodes, IP67 rated in accordance with IEC 62790
Cable:	4 mm ² solar cable, 0.9 m + 1.2 m in accordance with EN 50618
Connectors:	Stäubli MC4 PV-KBT4/PV-KST4 (4 mm ²) Tonglin TL-Cable 015-FR (4 mm ²) in accordance with IEC 62852, IP68 only when connected
Origin:	Made in Singapore

MAXIMUM RATINGS

Operational temperature:	-40 ... +85°C
Maximum system voltage:	1000 V
Design load (+): snow	367 kg/m ² (3600 Pa)*
Maximum test load (+):	550 kg/m ² (5400 Pa)
Design load (-): wind	163 kg/m ² (1600 Pa)*
Maximum test load (-):	244 kg/m ² (2400 Pa)
Max series fuse rating:	25 A
Max reverse current:	25 A

* Safety factor 1.5

TEMPERATURE RATINGS*

Nominal Module Operating Temperature:	44.6°C (±2°C)
Temperature coefficient of P_{MPP} :	-0.36%/°C
Temperature coefficient of V_{OC} :	-0.30%/°C
Temperature coefficient of I_{SC} :	0.066%/°C

* The temperature coefficients stated are linear values

MECHANICAL DATA

Dimensions:	1675 x 997 x 38 mm
Area:	1.67 m ²
Weight:	18.5 kg

Specifications subject to change without notice. Ref: REC-05-07-07 Rev. G.2 11.17

Founded in Norway in 1996, REC is a leading vertically integrated solar energy company. Through integrated manufacturing from silicon to wafers, cells, high-quality panels and extending to solar solutions, REC provides the world with a reliable source of clean energy. REC's renowned product quality is supported by the lowest warranty claims rate in the industry. REC is a Bluestar Elkem company with headquarters in Norway and operational headquarters in Singapore. REC employs more than 2,000 people worldwide, producing 1.4 GW of solar panels annually.


www.recgroup.com

Appendix B

Sunburn Repeatability Results from the flash test, for the floating module. The test was not run for the reference module.

Sunburn Repeatability Results

5100SLP BLUE

Module Type: ModuleType1

Module ID: 4005652604

Printed: 04/09/2018 10:54:21 AM

Intensity:	100.0 mW/cm ²
Monitor Cell #1 Conversion Constant	1.13 mA/(mW/cm ²)
Number of Curves Requested:	10
Number of Curves Completed:	10
Time Per I-V Curve:	26.00 s
Sweep Length:	100 ms
Sweep Delay:	10 ms
Sweep Direction:	Isc -> Voc

Meas.:	Average:	StdDev:	StdDev/Avg(%):	Max.:	Min.:
Voc	38.103	0.004	0.010	38.108	38.096
Isc	9.199	0.012	0.130	9.224	9.190
PMax	266.51	0.262	0.098	267.080	266.220
Vpm	30.82	0.05	0.162	30.889	30.723
Ipm	8.647	0.014	0.162	8.674	8.627
Ivld	0	0	0.000	0.000	0.000
Pvld	0	0	0.000	0.000	0.000
FF	0.76	0	0.000	0.761	0.760
Eff	16.152	0.016	0.099	16.187	16.135
Rs	0.472	0.019	4.025	0.509	0.450
Rsh	176.462	4.395	2.491	183.320	169.752



Norges miljø- og biovitenskapelige universitet
Noregs miljø- og biovitenskapelige universitet
Norwegian University of Life Sciences

Postboks 5003
NO-1432 Ås
Norway